J. Condensed Matter Nucl. Sci. 25 (2017) 26–55

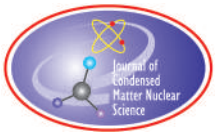

Research Article

Quasiparticles, Collective Excitations and Higher-order Collective Quasi-excitations in Lattice Assisted Nuclear Reactions

Mitchell R. Swartz*

Nanortech Inc., Wellesley Hills, MA 02481, USA

Abstract

Quasiparticles and collective excitations are similar in that they arise de novo from material interactions. They are in need of classification and important because some of them are highly relevant to successful lattice assisted nuclear reactions (LANR). This report reviews this classification along with discussion of their impact on our ability to enable LANR.
 ISSN 2227-3123

Keywords: Coherent excitations, Collective excitations, LANR, Phonons, Quasiparticle

1. Introduction– Overview

Knowledge of collective excitations and quasiparticles and their higher order coherent quasi-excitations helps in understanding the mechanisms occurring in both solid state lattices [1–5] and LANR [6–89]; and why the latter is requisite on the lattice.

Distinguishing quasiparticles from collective excitations and coherent excitations is critical. As a first approximation, these things are closely related. However, upon further examination, distinction between quasiparticles and collective excitations, which can be either coherent or incoherent, give much insight into what they are and their role in successful LANR. Furthermore, recognizing the existence of the higher-order collective quasiexcitations teaches the further relationship(s) of the new particle/objects to the real particle/object, offering further exploration of new physics and inventions.

1.1. Quasiparticles

"Quasi" means that something is seemingly or apparently something else that it resembles, but it is not really that thing. Examples in everyday life might include a shadow or one's reflected mirror image. These are quasi-objects which are the result of something producing something that was not there before.

*Dr. Mitchell R. Swartz ScD, MD, EE, E-mail: nanors@nanortech.com.

 ISSN 2227-3123

So in LANR and material science, quasiparticles are the first group of de novo particles/objects which are created by, and derived from, a real particle or object, or group of them when they interact with extended multibody systems such as a solid metal, or solid plane of glass, or other dielectric. Quasiparticles are induced by an interaction of the original particle/object and the induced quasiparticle, which are closely related things. The quasiparticles are similar to the "parent" real particles that create them, and appear as an "image" or a "reverse image" of the original particle/object that induced them.

The quasiparticle results from the interaction-at-a-distance of the original particle(s) with the surrounding solid polarizable and/or magnetizable material or lattice [1–5]. This follows a change in the material or lattice, sometimes called a "dressing", in response to the original particle. That word simplifies a highly complex environmental response which having atomic, ionic, orientation, and space charge, polarizations and several types of possible magnetizations.

And there are higher order effects. The end result is a new, real interacting particle/object appearing in space. This quasiparticle can itself react with other particles/objects/masses in space. For example, the changes can impact the particle's original electric (and magnetic) field(s). They are altered ("dressed", e.g., by "electric field screening") and thus, the particle and the environment are each effected by each other and changed. The solid can deform as well as electrically change from the alteration. Simply put, these changes comprise the quasiparticle, which has appeared in space as a response of the multibody stereoconstellation to the object.

Then there comes something new. The quasiparticle exists, and it can behave in a new, possibly anomalous, way.

1.2. Collective excitations

Collective excitations are the second group of de novo particles/objects. Unlike quasiparticles, collective excitations bear no resemblance to the constituent particle(s) of a real system that created them. Nor are collective excitations either the "image" or the "reverse image" of the original particle/object. Instead, collective excitations involve the appearance of an entirely new particle/object that is nothing like the original.

Unlike quasiparticles, a collective excitation involves an entire group, acting together as an aggregate (usually a lattice). Collective comes from the Latin "*collectives*" meaning "gathered together". They involve simultaneous motion of many physical particles linked together in space.

Collective excitations come from energetic reactions in a group of objects. An example of collective excitations include phonons, magnons, polarons, plasmons and excitons. But the best example may be the case of phonons, that is internal motion of the crystal lattice, itself.

Exactly how they are interconnected determines if the collective is coherent and "in phase" or if they are incoherent. Coherent comes from the Latin "*coherent*" meaning "sticking together".

1.3. Quasiparticles and collective excitations have real functional roles

The concept of quasiparticles and collective excitations are important to condensed matter physics because they can simplify incredibly complicated quantum mechanical, and macroscopic, many-body problems.

Some critics incorrectly purport without evidence that quasiparticles and coherent and collective excitations are not real. They are quite real and they actually produce many new properties of matter which are quite measurable, such as specific heat, as one example. The heat capacity of a solid crystal has contributions to energy storage from the phonons, and the excitons, and the plasmons, proving they are quite real, and not imaginary.

Furthermore, several of these particles have not been considered previously, and are associated with the metallic lattice [90–114], PdD_x, and the aqueous hydrogen lattice, D_2O [115–128]. Table 1 and Fig. 1 separate these objects/particles into several types, including higher order types, such as quasiparticles of collective excitations. The star (*) next to any name heralds that those quasiparticle/coherent/collective excitations facilitate or are associated with lattice assisted nuclear reactions (called also LENR, LANR, and cold fusion).

2. Background–Lattice Assisted Nuclear Reactions

Lattice assisted nuclear reactions (LANR) [6–89] enable deuterium fusion and perhaps other nuclear reactions and transmutations. The He^4-heat production manifold is incredibly clean and free of pollution, all toxic emissions, all carbon footprints, all greenhouse gases, and radioactivity, while obviating fossil fuel. The deuterium is plentiful in the oceans. Since 1989, most efforts for robust CF/LANR have failed because of a number of reasons, some which took years to understand, including flawed paradigms, cracked inactive palladium cathodes, contamination (including from ordinary water), improper cell configurations, and especially inadequate loadings (if measured at all).

Table 1. Quasiparticles, collective excitations, and higher-order coherent quasiexcitations.

A. Quasiparticles
(●) Electric Polaron – electron and its polarization cloud, including surrounding ions
(●) Magnetic Polaron – magnetic Moments organized as a magnetic polarization cloud
Exciton – bound electron and hole (absence of an electron below the Fermi level)
(●) L,D defect – quasiparticle enabling conduction in aqueous systems
B. Collective excitations
(●) Phonon – collective of mechanical vibrations arising in a lattice
Plasmon – collective excitation (quantum) of plasma oscillations
(●) Spin-wave magnon – collective excitation of electrons' spin magnetic moments in a lattice
C. Higher order quasiparticle enabling collective excitation or de-excitation
Exciton–polaritons, phonon–polaritons, and plasma polaritons
Mössbauer-effect couples the entire lattice to a nucleus
(●) Nanoron – magnetic quasiparticle in magnetized dry preloaded NANOR-type CF/LANR components which produce a second optimal operating point (second pathway) amplifying incremental power gain significantly.
(●) Phuson high impedance PHUSOR-type CF/LANR system amplifying incremental power gain significantly.
Plasmariton – optical phonon and dressed photon consisting of a plasmon and photon
Spinons – observed as quantum spin fluids in Herbertsmithite
(●) Indicates that this plays a role in lattice assisted nuclear reactions.

As always, experiment-derived facts rule. The experimental facts show that LANR research is quite real, and its history shows that it is developing. That development now involves many types of CF/LANR systems. These include the original aqueous electrolytic systems [6–64], which now have a variety of types, ranging from conventional (F+P) [19–22], to electrolytic systems (with solution resistance ranging from conventional to "high impedance" devices in the range of 200,000 Ω or more) [12,13,33–47], to two types of codeposition (JET Energy vs. SPAWAR and Miles) [12,13,49–64]. There are also several nanomaterial systems including preloaded LANR components [65–79], and gas permeation loading [80–82], dual cathode systems [70], ion beam, glow discharge loading cells and other systems [83–87].

They run in both open and closed systems, and driving motors, with on-line monitoring, redundant, high precision, time-resolved semiquantitative calorimetry [13].

Several LANR devices show excess power gains from 25% to many times input electrical power. The preloaded Nanortech nanomaterials show incremental power densities of circa 19 kW/kg [6,73,74].

JET Energy Inc. has shown that some aqueous electrodes, of specific shape, are metamaterials which produce excess heat of a superlative magnitude, successfully driving Stirling engines at the 1–19+ watt excess power level [6,12,13]. In 2003, JET demonstrated a working LANR high impedance PHUSOR-type LANR systems for five days at MIT at ICCF10, producing ∼230% excess energy at 1–2 W level [39,6]. Such new LANR technologies, linked helium-4 production [7,11,65], increasing power gains and total energies achieved since 1989, are all paving the way

	Schematic Drawing in Material and LANR Science	Metaphorical Representation
Quasi-particles	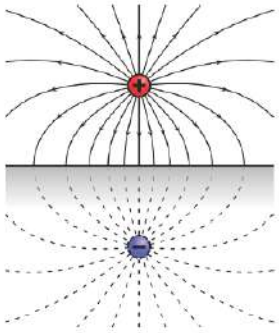	
Collective Excitations (Coherent or incoherent)	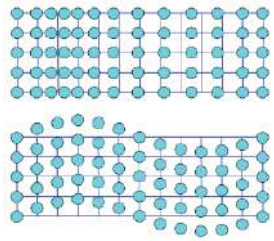	
Collective Coherent Excitations	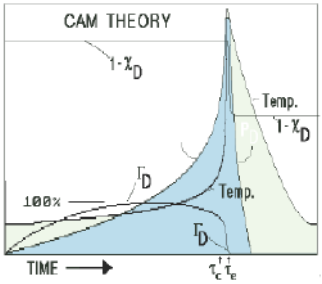	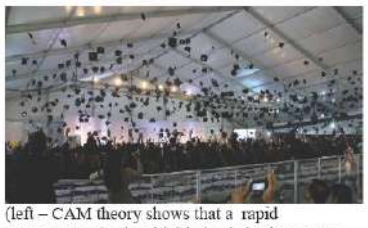 (left – CAM theory shows that a rapid temperature rise in a highly loaded PdD system can initiate catastrophic changes, including deloading and internal deuteron movements)

Figure 1. Schematic and metaphorical quasiparticles and collective excitations. The schematic drawings and the metaphorical representations both show the relationships between quasiparticles and collective excitations and coherent excitations. The first row represents a charged particle and its mirror-image quasiparticle. The second row shows compressional and transverse phonons which are collective excitations. The third row shows catastrophic release of D_2 in suddenly heated, loaded PdD. On the left are graphs and schematic cartoons that attempt to visualize a small portion of a very complex material science stereoconstellation. On the right are the metaphorical representations.

to an important, new, clean form of energy production: LANR.

2.1. LANR/CF is consistent with conventional physics

LANR/CF is consistent with conventional physics, and analysis of the quasiparticles and collective excitations requisite for success demonstrate that. But successful LANR remains very difficult to achieve. The first key for successful LANR is that the PdD_x alloy must be driven, usually electrically, to extremely high loading, until it is filled and

almost saturated like a sponge with water, and near-bursting like an over-filled balloon. The electrode must accept and maintain high loading for excess heat (>90%), for a sufficient incubation time, up to several hundred hours [6,88,89].

Why? Vacancies must drift into the bulk from the surface, energetically facilitated by the loading itself [6,129,130]. The vacancies are the site where the desired reactions occur. The vacancies must be formed, diffuse in, and be filled before the material is destroyed. The additional, difficult to achieve, keys for successful LANR, is that there must be integrity of the loaded alloy. This is a condition which is circumvented to some degree by the codeposition methods, albeit with their limitations [55].

The dynamic control is complicated. As the lattice loads, it swells. Too much swelling yields irreversible failure, just as a burst balloon.

The fuel for LANR is the deuteron. The deuterons are driven onto the surface of the metal by the applied electric field intensity, using electrochemistry [131–134], or by gas pressure applied. They diffuse and are driven into the metal, sometimes being driven into the vacancies, especially by the Catastrophic Active Media (CAM) reactions (described by the CAM theory; discussed below [135,136]).

In LANR, excess heat and He^4 [7,11,65] are the usual products, and tritium [8–10], charged particles, gamma radiation and the sequelae of neutrons [50, 52–54,66,67] can be sometimes detected.

Melvin Miles of China Lake with Johnson–Matthey Pd rods was the first to show the correlation of heat and He^4 production. Arata and Zhang reported de novo He^4 with LANR, including with Zr_2O_4/Pd powder exposed to deuterium gas, but not with hydrogen gas. Les Case using LANR with platinum group metals on carbon catalysts, reported He^4 production from deuterium gas.

As a result of these findings, but ignoring the intermediates and the impact of the lattice for the moment, the reaction is something like

$$D + D \longrightarrow H^4 + \sim 22\ \text{MeV(lattice)}. \tag{1}$$

In most cases, the product is an extraordinary amount of heat. That product is created at above-normal levels of electrical dissipation, called "excess heat". The LANR-derived "excess energy" begins at high energy, in the excited state of helium, which is obtained from reactions between deuterons within the lattice. That He^4 excited state is either the first excited state, or one energetically located above it, all at least 20 MeV (20 to ∼23+ MeV) above the ground level. This is significant in magnitude and clearly not "low energy", as often (mis)claimed. As such, purported "low energy nuclear reactions (LENR)" are a misnomer, a paradoxical description of what is actually not observed. Fortunately, they are high energy reactions. An actual LANR sample comprises a population of $\sim 10^{20}$–10^{22} candidate nuclei (among deuterons at ∼1:1 ratio) which if active fuses $\sim 10^{12}$ deuterons/s for each 1 W of excess heat produced. The mechanism will be discussed below, with consideration of the CAM and PHUSON coherent excitations, as Eq. (1) is greatly expanded.

2.2. Lattice assisted nuclear reactions may occur at different locations

Three regions are postulated as potential LANR sites. This (called "3RH") is suggested by existence of three optimum operating point (OOP) manifold groups – known to characterize all LANR systems [33–36,137–143]. It is heralded by, and also consistent with, some experimental data, including our report of (at least) two time constants characterizing "heat after death" (HAD) excess heat [31,43,44]. We previously reported at ICCF10 and thereafter, that the loaded active palladium lattice's deuteron-loading capacitance is ∼64 mmol/V*. The systems' admittance for the desired excess enthalpy (measured during "heat after death", also called 'tardive thermal power (TTP) reactions'), is ∼7 pmol/s-V* and that capacitance is dwarfed by the system's deloading admittance for loss of deuterons during outgassing which follows turning off the electric field intensity, and that is ∼15 nmol/s-V*. The kinetics reveals HAD evanescent heat generated by two (or more) sites [43,44]. Most of the sites have TTP which falls off with a time constant of several

minutes, but some of the sites had a time constant of ∼20 min to hours. This is consistent with vicinal surface and deeper sites, with the longer time constant associated with the deeper location within the lattice.

The three different regions of physical locations distinguished are: Region 1 involves the most superficial portions of the palladium, including surface dendrites and a variety of micro- and nano-particles, that characterize electrodeposited, and codeposited palladium alloys involving and at least several atomic layers. These surface sites, generated via codeposition and conventional LANR produce tritium [8–10,49]. Located deeper in the metal, subsurface Region 2 is the metallic lattice physically located beneath Region 1, existing as a thin rim under the surface in the range of 40 mμ to mm. Subsurface sites (Region 2) yield heat and helium production and transmutation products [7,8]. They characterize conventional LANR ("FP") systems which make excess heat with commensurate helium production in palladium with heavy water, and excess heat with nickel systems in both light and heavy water.

Region 3 represents deeper sites, or spatially, deeper sites in the metallic lattice or palladium-black systems which efficiently yield heat and helium production. Region 3 is less commonly involved in LANR, perhaps only in the very rare reports involving ("paroxysmal") energy release from larger volumes. It appears to be involved with Arata's palladium black in dual cathodes and the NANOR-type preloaded LANR components. These three regions have been analyzed. We corrected, and expanded Nagel's surface monitoring equation [85] to the modified, volume-corrected, multi-site, Excess Power Generation (EPG) equation [36] for use with OOP manifolds [33–143]. The EPG is shown in Eq. (2) is a double summation (or double integral) where the summation is over each of the three regions, and over depth within each region. The area is A. *E* is energy per reaction and XSE is the excess energy, so dividing it by the time, *T* yields the excess power, XSP.

$$\mathrm{XSE}/T = \Sigma\Sigma[[A * (\text{depth})] * F_{\text{vol}} * [N/(A * \text{depth-sec.})] * F_{\text{theor}} * E] = \mathrm{XSP}. \tag{2}$$

Summation occurs over each of the sites (or layers), in the surface, subsurface and deep volume. The first term on the right hand side of the equation is the actual volume involved with active foci, followed by the fractional active palladium sites with defects, etc., as required, within that volume, followed by the reactions per second at each of those sites within that volume, and finally a theoretical term (between 0 and 1).

E is the energy per reaction (circa 24 MeV per fusion reaction from the estimations of Miles, McKubre, and Apicella/Violante [6,7,11, 114], or perhaps 2 MeV less based on the theoretical considerations [161]). F_{vol} is the functional number of the volume of each site (or layer). It could be 1, or less if the nucleus required is blocked from entry (e.g., deuterons blocked by hydrogen). N is the LANR reaction density, or the number of reaction sites per A, by layer. If N are taken as the vacancies, they may vary at the different regions, such as being very high in the codepositionally created volumes.

In the equation, F_{theor} represents several factors that control, or throttle, the coupling of the He^{4*} to the lattice. When it varies from 0 to 1, it can thus handle the Coulomb barrier problem by using several theories and factors [144–166], the most important of which will be discussed below. Some factors might relate to needed loss of the de novo helium-4 generated from the active sites, which might be much higher near the surface region than in the bulk region. Other factors may include magnetic interactions such as have been reported with dry, preloaded NANOR-type systems [79].

If the active sites are taken as vacancies, for normal Pd and some PdD levels, this has been investigated by several means, including discussion of the Fukai state which is the maximal level achievable experimentally, and the "healing" that occurs as the lattice tends to reform from those peak vacancy states [129].

3. Electric Polarization and Electrical Conduction

Electrical polarization is ubiquitous. All materials are characterized by their response to an applied electromagnetic field. The applied electric field intensity, E, results in an electrical conduction within the material, and via the electrical

conduction process (and there may be many), there follows the linked electrical polarization. It is these polarizations (ionic polarization, atomic polarization, orientation polarization, space charge polarization, and domain polarization) which make each material unique.

Electrical conduction and polarization are, and must be, related because any motion of charged particles, and of molecules with distributions of charge, necessarily result in both conduction and subsequent polarization as a result of the motion. As a result, these two aspects of the complex permittivity are also related through the Hilbert space.

There are many types of electric polarizations. Electric polarization is very important because of the many ways it relates to LANR (and so much else). For example, other electrically charged particles also induce polarons, including from deuterons, when they are loaded in the palladium or nickel cathodes

3.1. Role of frequency and E-field intensity

Figure 2 shows the types of electric polarizations that can occur. Notice that fewer types of electrical polarization become available at increasing frequencies. This falloff of contribution occurs because heavier masses cannot keep up with the driving frequency of the applied electric field intensity at higher frequencies.

As Fig. 2 demonstrates, the complex dielectric permittivity is a function of frequency. At low frequencies, the induced ("second-order") magnetic field can be neglected and so what is important is only the response of material to an applied electric field intensity. That said, it is also important to recognize that the E-field may be quite large locally. Depending on the materials, solutions, and electrodes, if irregularities are present at an electrode, for example spikes on a cathode, and if charge carriers are present in the solution, then the electric field intensity distribution can change dramatically with tens of thousands of volts per centimeter suddenly appearing over, or near, such irregularities.

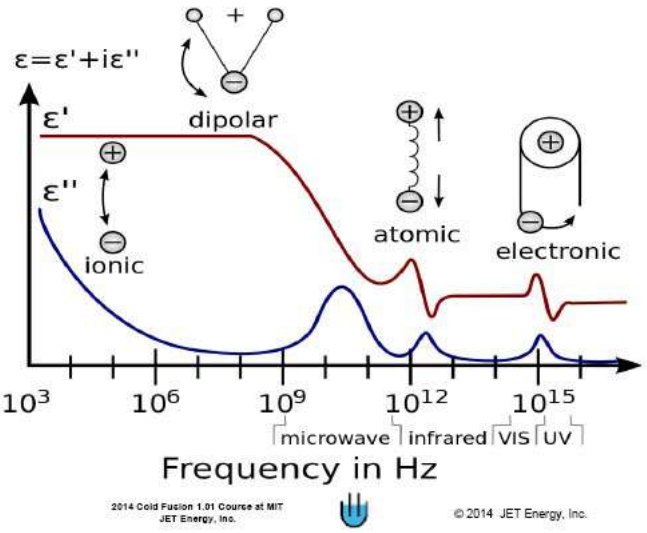

Figure 2. Real (ε') and imaginary (ε'') parts of the complex dielectric permittivity of a hypothetical material as a function of frequency. Shown are four types of electrical polarization. Each polarisation/conduction has an imaginary contribution, with a peak, (*blue curve*) adding to the electrical conduction. From von Hippel "Dielectric and Waves" [124].

3.2. Complex relative permittivity

From a mathematical point of view, the electric polarization (κ') is the real part of the complex relative permittivity (κ*).

$$\kappa* = \kappa' - j\kappa'' \tag{3}$$

ε'_0 is the permittivity of a vacuum. When the permittivity of a material, ε is divided by ε, the result is κ' which is the relative permittivity. This is called the "dielectric constant", However the term "dielectric constant" is itself a misnomer because it is not a constant, but changes with, and usually decreases with, frequency. That said, for most materials only electric and ionic polarisation are significant, and therefore the dielectric constants of almost all materials, except ferroelectrics and water/ice (vide infra), are usually in the range of 3–6.

The electrical conductivity of a material is mathematically described by the imaginary part of the complex permittivity and is the product of the electrical conductivity and the angular frequency.

$$\kappa'' = \sigma * \omega. \tag{4}$$

4. Quasiparticles

A quasiparticle generally results from the interaction of a constituent particle with the surrounding solid polarizable or magnetizable material. Several types of quasiparticles are described in this section.

4.1. Electric polaron – Electron and its polarization cloud, including surrounding ions

Perhaps the simplest example of a quasiparticle is the "electron quasiparticle" or "polaron". A polaron is a quasiparticle which comes about when an electron (and its surrounding electric field) interacts with its surrounding ions, which may be free to move, and then distorts the stereoconstellation of those positive and negative ions around it.

First, the important point here, for this moment regarding polarization (including in water), is that quasiparticles can be induced. For example, if and as the electron moves, the surroundings are perturbed in complex way producing a sort of tunnel through which the electron can move. Attention is again directed to the fact the differences between the real free electron particle, and the one moving through a lattice, driven by an applied electric field, as an electric polaron quasiparticle is created. In the latter, the electron behaves as if it had a different, heavier mass due to exchange and correlation interactions with all the other charged particles, despite their having the same charge and spin.

4.2. Magnetic polaron – Magnetic moments organized as a magnetic polarization cloud

Magnons can be created as two types of quasiparticles and one type of collective excitations. First, one magnetic quasiparticle occurs as the L and S moments (angular magnetic moments of electrons in atoms) couple as J, and as described in quantum chemistry. Thereafter, second, the single magnetic moment is oriented and can magnetically polarize the lattice or environment around it. This is the magnetic equivalent of the electric polaron. However, although the impact on the medium is similar, the interaction forces are much weaker.

4.3. Exciton – Bound electron and hole (absence of an electron below the Fermi level)

What is a "hole"? It is the absence of some material, particle, or object (Fig. 3). Consider a pearl falling into a thick shampoo solution (e.g. from the 1960s Prell shampoo commercial, https://www.youtube.com/watch?v=9lFsrjoLKq0).

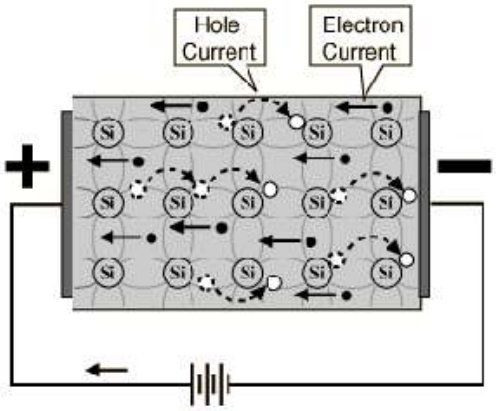

Figure 3. Schematic of the electrical conduction through a semiconductor material driven by a battery. Holes and electrons both contribute to electrical conduction.

The flow analysis can either be based on Eulerian coordinates simply following the flow of the fluid around the pearl (requiring solution of the fluid flow as a $f(x, y, z, t)$, first, and using the convective derivative) OR based on Lagrangian coordinates following the transit through the thick solution (with the location of the pearl as a $f(x, y, z, t)$). The latter is much easier to calculate. In solid state physics, a hole similarly consists of a missing electron from the valence band of the crystal semiconductor. The hole is a quasiparticle in the "reverse image" of an electron, and it can interact electrostatically, much like an electron. That is because the hole is functionally and relatively electrically positive, opposite the charge of the electron. Thus, the hole can interact electrostatically with the electron and even produce a bound state with a measurable binding energy. The interaction creates yet another quasiparticle, the "exciton", which results from the bound electron and hole and their interactions, together.

4.4. L,D defect – The quasiparticle enabling conduction in aqueous systems and the loading of Pd and Ni

The hydrogen-derived quasiparticle, and particularly relevant here, the deuteron-quasiparticle, must be considered because they each create L- and D-defects in heavy water, and their ferroelectric inscription patterns. This is one of the most important quasiparticles in CF because it is THE origin of the fuel for LANR via the deuteron to He^4 fusion reaction for most aqueous CF/LANR systems, such as the classic F–P system, the codepositional, the high impedance, and PHUSOR®-type system. In each of these, the deuteron is driven into the metal by the applied electric field intensity.

In most cases the product is gas evolution, and in successful CF/LANR there is also produced an extraordinary amount of heat and nanoscopic quantities of *de novo* He^4. Understanding this important quasiparticle begins with the requirement of considering the structure of water and, therefore, ice.

4.4.1. *The nano-structure of water – There are two lattices in water and ice*

Water is not a gas but has a three-dimensional stereoconstellation, and surprisingly it has both elements of order (the oxygen atoms) and disorder (the protons or deuterons).

Water's atoms of oxygen and hydrogen (or deuterons) are arranged in structures with definite physical rules and it is best understood as a complicated three-dimensional structure comprised of two lattices. The lattice of the protons

and/or deuterons is located within a second lattice (the oxygen atoms). The most important point is that *there are two lattices* and that the proton lattice is often totally ignored. Much has been learned by studying the protons, their electric dipole moments, and their entropy, which result from their distribution and decoration upon the organized oxygen lattice.

The fact that water has a second proton lattice within it means that water has not only singular properties, but has an incredible impact upon both the properties of materials dissolved within it (including clathrates, hydrates, biological systems, etc.) and the operation of systems using it. Additional complexities occur because the hydrogen in water could be the rarer heavy hydrogen, deuterium, which is the desired fuel in CF/LANR and is used at the 98–99.95% levels in the best CF/LANR systems.

4.4.2. *The organized oxygen lattice*

Water is actually two lattices [115]. First, there is the spatially fixed oxygen lattice, which is a hexagonal lattice (Wurtzite type). It is an ordered lattice and is "decorated" by a second proton lattice, which is disordered in ordinary ice (Ice 1_{h}).

Deuteron Bond/Hydrogen Bond – Etiology of the Ordered Oxygen Lattice

The origin of the oxygen lattice of water begins with electronegativity of the oxygen atom. That electronegativity creates asymmetry by the displacement of the electron clouds toward the oxygen atom. With that resultant asymmetric redistribution of electronic charge within the water molecule, there then follows the creation of unbalanced (positive) charges at the hydrogens (or deuterons) and negative charges in the form of two "free" (negative) sp^3 lobes surrounding the oxygen nucleus and creating the tetrahedral appearance.

The H-bond process immerses a proton into an electronic cloud of a second neighboring water molecule, creating one hydrogen bond by neutralizing charge. The Coulombic neutralization is large, and on the order of 4.5 kcal/mol (compared to the relatively much less "background thermal energy" which is only $k_{\mathrm{B}}T =\sim 0.6$ kcal/mol) making the hydrogen bond thermally stable.

This asymmetric charge redistribution produces both an intramolecular dipole moment, and most importantly can result in a "hydrogen bond" (or "deuterogen bond") by having two (or more) water molecules self-assemble. These hydrogen bonds are ubiquitous, partially due to the low steric requirements of the protons (from the ability to rotate). Then, something wonderful happens.

The water molecules are linked by hydrogen bonds into a complicated tetrahedral system locally and regionally. First, the structure of water and ice on the atomic scale is associated with tetrahedral symmetry from the orientation of the oxygen atom (Fig. 4). Each water molecule is engaged in four hydrogen bonds. In two, the hydrogen atoms are about 1 Å from the origin, whereas the other two hydrogen bonds have hydrogen atoms from neighboring water molecules which are more distant. This difference is critical and creates the electric dipole moment and the proton disorder [115–128].

4.4.3. *The disordered deuteron lattice*

The proton disorder of water's hydrogen sublattice leads to the unusual electric conduction and polarization properties of water. Most importantly, the proton disorder creates the large dielectric constant of water that enables water to dissolve so many materials. Furthermore, the proton disorder of water/ice contributes to the great heat capacity of water (the ability to absorb heat with a negligible increase in temperature).

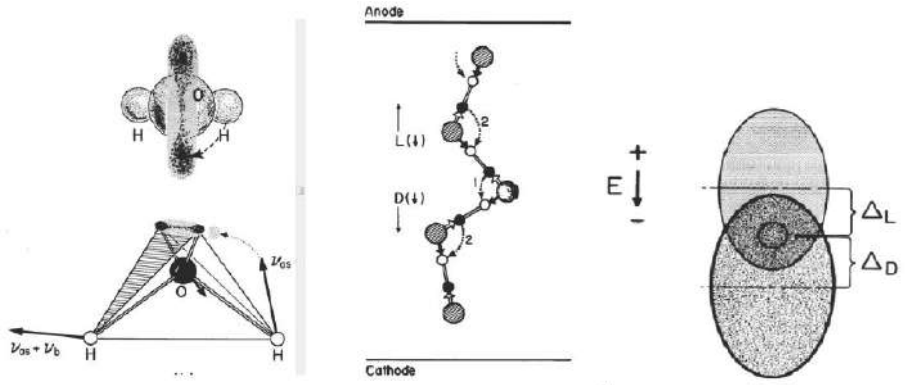

Figure 4. (*Left*) Water's tetrahedral structure permits intramolecular proton transfer making L and D defects. L- and D-proton defects initially arise from infrared vibrations. Here one such vibration launches a proton from one oxygen electron orbital to another creating the paired defects. (*Middle*) The diffusion of L, D defects inscribe ferroelectric dipole moments recorded by dielectric spectroscopy. (*Right*) an applied E-field makes L and D defects move through the lattice and creates drift ellipsoids of leaving the inscribed ferroelectric polarization, from these quasiparticles, onto the aqueous lattice (seen macroscopically).

4.4.4. *The macro-structure of water*

How is water like ice? In water, only about one-seventh to one quarter of the hydrogen bonds are broken compared to fully frozen ice. This can be quickly shown as follows. Consider the ratio of the heat of fusion (which is what takes ice to water) to the heat of vaporization and fusion and two other terms. The first additional term in the denominator is the 100 calories required to reach 100°C. The second term arises from the fact that ice is not truly a solid (consider the surface during skating) until –30°C, which adds yet another 0.5 cal/g-°C of the material to the denominator. This ratio supports the details and conclusions outlined above, that the only correct conclusion is that the majority of hydrogen bonds in water are intact.

The structure of water appears to be a mixture of Ice 1_h (50%), Ice 2 (30%), and Ice 3 (15%). Probably much more subtle variation exists, and certainly so near any electrode, double layer, and/or energy system. Ice 1_h is the hexagonal form of ordinary ice, ubiquitous on Earth. By contrast, Ice I_c the metastable form characterized by cubic symmetry, and only obtained at high pressure.

4.4.5. *Large dielectric constant of water and ice*

For most materials the dielectric constants are usually in the range of 2–6. However, for water and Ice 1_h, the arrangement of the molecules permits proton disorder in the sublattice and thus introduces a new method of electric conduction and polarization (Figs. 4–6), and the result is a much larger dielectric constant; a whopping 92 for ice, and 88 for water [115,126–128].

The unusually large dielectric constant (= the real part of the complex permittivity) of water is particularly important because it both distinguishes it from most other materials and because it enables diverse reactions ranging from chemical solvation to free radical reactions, which can then occur by shielding free charge and unpaired electrons, respectively.

It is water/ice's proton disorder and the drift of L,D defects which creates the unusual dielectric properties of water.

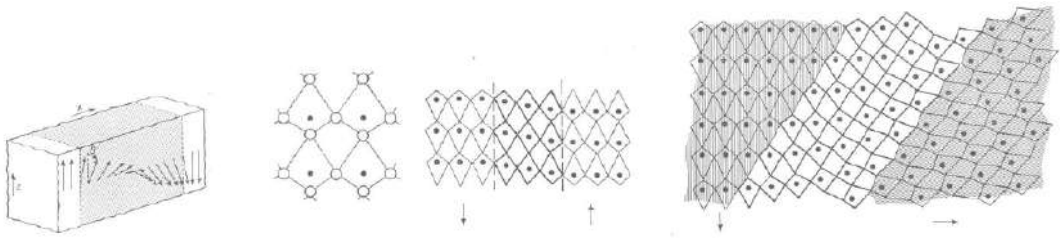

Figure 5. Spin wave magnons can quantum link regionally different domains of magnetic polarization in a lattice. Here they are shown schematically (*above*) as a spin wave; and (*below*) as the domain representations showing the domain shears.

4.4.6. *Deuteron disorder and L, D defects*

Normally. there is one proton between each pair of oxygen nuclei (Fig. 5), but not always. L and D defects initially arise from infrared vibrations, as suggested by Bjerrum (Fig. 6). A D-defect has two protons between any two oxygen nuclei. An L-defect has none.

Thus, with sufficient background thermal energy there are created many L and D defects throughout the volume of water or ice. Then, the action of an applied electric field intensity to that sample of water/ice results in an electrically induced drift of these intramolecular proton (and deuteron) defects.

4.4.7. *Conduction/polarization phenomena – L, D defects quasiparticles and their diffusion*

The result of an applied electric field on the L- and D-defects is that the E-field inscribes a series of intramolecular defects into the water lattice (cf. Fig. 4). The inscribed defects create a large electric dipole moment.

Over vast distances, the L- and D-defects migrate in an applied electric field intensity. The normal spheroids of defects distort into field-directed ellipsoids, which are shown. As the defects migrate, they leave trails of proton order which are slowly erased by thermal action. Their movements inscribe into the proton sublattice a generally field directed electric dipole moment, as von Hippel and others at the Laboratory for Insulation Research (MIT) have shown.

It is this inscribed electric dipole moment which creates the large dielectric constant. Those who work with cold fusion and energy conversion systems involving water ought to consider these defects, referred to above, which markedly impact the proton disorder and the characteristics of water and ice.

In heavy water, the small ratio of electrical energy compared to k_BT, produces drift ellipsoids of L- and D-deuteron defects. This yields a cathodic "fall" of deuterons, a double layer in front of the electrode surface. The concentration polarization produces very large local electric field intensity, ranging from 10^4 to 10^7 V/cm [131,5]. The double layer is a relaxation response, and not a resonance response. Transfer of deuterons through it can be enhanced by light [42], however.

In summary, the applied electric field intensity causes E-field directed movement of the quasiparticles formed of the defects. The high dielectric constant of water actually results from movements of protons in and through the proton lattice creating a ferroelectric inscription with several important implications.

4.4.8. *Dielectric spectroscopy of water/Ice*

These phenomena are observed and measured by dielectric spectroscopy. Dielectric spectroscopy is the study of a material's electrical properties as a function of frequency. When water is examined by AC electric fields, from approximately 8×10^{-3} to 10^7 Hz for ice, higher for water. There are resolved several complex dielectric relaxation

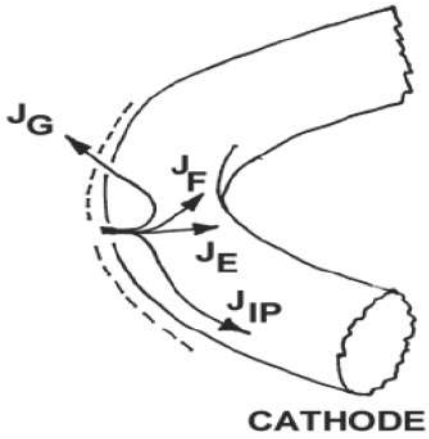

Figure 6. Schematic showing the deuteron flows at a cathodic electrode metal surface. The solution is to the left. At the metal surface, several components of deuteron flux must be considered; entry into the metal (J_{E}), movement to gas evolution (J_{G}), and an extremely tiny loss by potential fusion reactions (J_{F}). J_{IP} is a pathway afforded with a metamaterial [163].

spectra resulting from the proton sublattice and the movements of L- and D-defects (e.g., confer Fig. 6). Even the "purest" Ice 1_{h} has seven (7) discrete subspectra (not all are seen in Fig. 7). More information is in IE [115] and von Hippel's texts [126–128].

The largest ("major") subspectrum (previously, formally called spectrum #3) of water and ice is most related to the classic "dielectric constant." It does not result from water molecules spinning like tops as is popularly supposed. Also it does not result from rotation of the water molecules, as is also popularly supposed. In fact, it could never

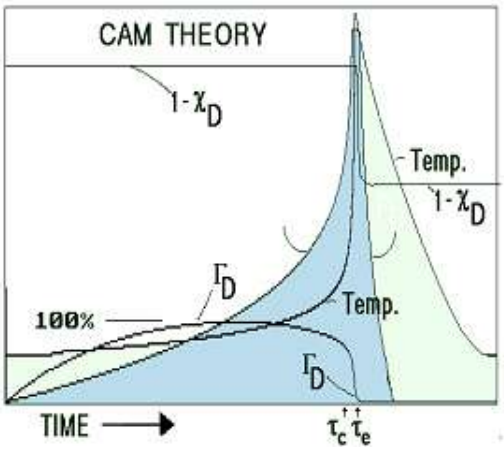

Figure 7. This graph shows the theoretic results of a sudden catastrophic active media (CAM) desaturation of a palladium electrode with respect to deuterons. As the palladium heats up (in positive feedback), the solubility of the D in it decreases, leading to a massive falloff of the fractional saturations (D/(PdD) % defined as Γ_{D}). This drives the deuterons by the CAM catastrophic desaturation into the vacancies which are the site of the LANR reactions. The time constants, τ_{C} and τ_{e} , and the other variables, are discussed further in the original paper [135,136].

result from either because the ratio of the hydrogen bond energy to the thermal energy is so large that the bonds are stable. Simply put, the structure of water and ice are too energetically bonded and energy-expensive to enable the l3.5 kcal/mol required for any such rotation, or the 18 kcal/mol required to rip a water molecule out of an intact lattice.

Hence the high boiling point of water. By contrast, the high dielectric constant of water actually results from movements in the proton sublattice, that result from the electric field-directed movement of defects in the proton sublattice.

5. Collective Excitations

In contrast to quasiparticles, collective excitations result from aggregate behavior (of the lattice, or dielectric, or even plasma) and bear no resemblance in any way to the aggregates components and constituent particles. Some involve motion of many physical particles linked in space, like phonons or plasmons, that are from atomic and electronic motions within the crystal lattice, itself.

How they are connected determines if it is simply incoherent collective, or truly coherent collective excitations.

5.1. Collective excitations – Phonons – Quantizations of mechanical lattice vibrations

The first example of a collective excitation is the phonon. A phonon results from the coherent vibrational motion of the locoregional periodic atoms comprising the crystal lattice. Phonons occur widely because all lattices, in which the energy is invariant under a rigid translation of the entire lattice, must have at least one acoustic mode (sound wave) with resultant collective, coherent, oscillations of the crystal lattice. Unlike fermions, phonons are bosonic quantized lattice vibrations meaning that an arbitrary number of phonons can be excited in each phonon mode.

In successful LANR, there are enough phonons (lattice vibrations) to act coherently, to enable coherent energy transfer (from where the excess heat arises for the just-formed high energy helium excited state to shed $\sim$20+ MeV to the lattice [6,144–147,149,156–162] as the He^4* returns to the He^4 ground state. Hence the "excess heat". Ergo, it is the lattice – and specifically phonons – that open up the new pathway.

5.2. Collective excitations – Plasmons – collective excitation quantum of plasma oscillations

Plasmons are the quanta of plasma collective oscillations and excitations. They can occur both in lattices and in electron gases and plasmas where all the electrons oscillate synchronously with respect to all counter-ions via Coulomb interactions. Plasmonics goes even further and uses optics and nanoelectronics to make novel devices. However, present plasmonic devices suffer from ohmic loss and electron-core interactions [177].

5.3. Collective excitations – spin-wave magnon in a lattice

Spin wave magnons are quantum magnetic spin waves collectively excited in the crystalline lattice. They exhibit new degrees of freedom as they arise from the interaction of the electrons' magnetic spin structure (already a quasiparticle) with the crystal lattice within which it sits. The result is the quantum spin wave (Fig. 5) [178,179].

6. Higher Order Quasi-particles of Collective Excitations

Unlike quasiparticles, collective excitations result from the ORGANIZED aggregate behavior within the object (usually a lattice). A coherent collective excitation is one which is united and forms an entire uniform constant phase relationship.

Examples are given in Table 1 and below.

6.1. Quasiparticle avoiding collective excitation – Mössbauer effect

The first example is the Mössbauer effect [167–175] which works by coupling iron nuclei in the crystal lattice by with the iron atoms' electronic s-orbitals. The Mössbauer effect is recoil-free emission and absorption of gamma radiation by a nucleus contained in a solid lattice. Although momentum is conserved, the entire lattice coherently is involved in the excitation and/or de-excitation. In the Mössbauer effect, the lattice as a whole recoils and thus the recoil energy is very well defined with no phonons involved, and thus (inaccurately) called "recoil-free". Importantly, this leads to very narrow line-widths (with a Q of $\sim 10^{14}$ vs. a laser with a Q circa 10^{10}). This is important to CF/LANR in that it absolutely demonstrates the existence of nuclear coupling to the lattice by demonstrating conclusively that the nucleus is connected to the lattice through the s-orbitals, which do not go to a probability of zero at the nucleus.

6.2. Complete theory of CF/LANR

6.2.1. *Quasiparticle enabling collective de-excitation*

Successful LANR begins with loading of the lattice, the kinetics of which can be described by the quasi-1-dimensional model of loading. LANR, after loading, then has at least two coherent excitation/quasiparticles in its successful action. These sections will describe the pathway to successful activity in LANR. What is described here is a multistep process to LANR.

Then there occurs a coherent excitation involving the catastrophic active media forming deuteron flux and very rapidly filling of the vacancies (CAM theory). Under some circumstances, as discussed by Takahashi, Scott and Talbot Chubb and others, there can occur in the lattice the formation of excited helium 4 (^{4}He*). Finally, in the fourth irreversible step there is the de-excitation through the PHUSON coherent particle [161]. These steps, and the energy levels explain the observations of LANR – including the excess heat, and the lack of significant emissions.

6.2.2. *CF/LANR first requires loading*

As discussed at ICCF-4, we suggest a series of reversible reactions which lead up to a final irreversible step. The series includes an intermediate state which is called apo-^{4}He* (meaning that which occurs before the ^{4}He* is seen). apo-^{4}He* is on the way to becoming the excited helium state, ^{4}He*, located about 22 MeV above the ground state of helium. If the conditions are perfect, ^{4}He* can then become de novo ^{4}He and heat the lattice, where it appears as "excess heat". If successful, then in the highly loaded lattice (n D within the Pd, which is ignored in this equation):

$$\text{n D} \Longleftrightarrow \text{apo} - {}^4\text{He}^* \Longleftrightarrow {}^4\text{He}^* \longrightarrow {}^4\text{He}. + \text{“excess heat”}. \tag{5}$$

Step 1 – (a reversible step) Loading of palladium by deuterons

The LANR reaction begins in the extremely difficult-to-achieve highly loaded Group VIII lattice. There is a critical content of loaded Pd for activity, generally described as a requirement of $>\sim 0.85$ (McKubre, Tanzella and others [6]). Understanding this system requires continuum electromechanics and not electrochemistry.

6.2.3. *CF/LANR requires deuteron flux*

Deuteron flux is examined here by the quasi-1-dimensional model of loading which shows that conventional "electrolysis" is WRONG and a "red herring", and is why many have trouble achieving successful LANR. The Q-1-D equations [140,141] show the way to optimal results. These equations explain some of the difficulties $\sim$1989+ and they DO NOT DEPEND upon equilibrium conditions, and in fact they make successful predictions (both unlike the relatively useless Nernst equation).

Figure 6 shows a metal surface and several components of deuteron flux. They must be considered, including entry into the metal ($J_{\rm E}$), movement to gas evolution ($J_{\rm G}$), and an extremely tiny loss by potential fusion reactions ($J_{\rm F}$). $J_{\rm IP}$ is a pathway afforded by the high impedance spiral PHUSOR-type LANR component (not to be confused with the Phuson).

$$J_{\rm D} = -B_{\rm D}\frac{{\rm d}[D(z,t)]}{{\rm d}z} - \mu_{\rm D}[D(z,t)]\frac{{\rm d}\Phi}{{\rm d}z}. \tag{6}$$

Equation (6) describes the flow. $J_{\rm D}$ is the flux of deuterons, $B_{\rm D}$ is their diffusivity, and $\mu_{\rm D}$ is their electrophoretic mobility. The deuterons can enter the metal forming a binary alloy. Deuterons which enter (load) into the palladium lattice drift from shallow to deeper sites within the palladium, obstructed by ordinary hydrogen at interfaces and grain boundary dislocations. The quasi-1-dimensional model begins with the Navier–Stokes equations which ia also used to describe flow for fluids and other materials in continuum electrodynamics [5].

Dividing each flux by the local deuteron concentration yields the first order deuteron flux constants, $k_{\rm E}$, $k_{\rm G}$, and $k_{\rm F}$ (cm/s), respectively. They are linked as follows through Gauss' law and integral equations.

$$k_{\rm E} = \mu_{\rm D}\, E - (k_{\rm G} + k_{\rm F}). \tag{7}$$

This shows absolutely clearly that LANR can be missed by insufficient loading, contamination (affecting $k_{\rm E}$, e.g. by protium), and by the evolution of D_2 gas, which all inhibit the desired reactions. This also shows that the first order deuteron loading rate equation teaches that the deuteron gain by the lattice depends on the applied electric field *MINUS* the loss of deuterons from gas evolution ($k_{\rm G}$) and fusion ($k_{\rm F}$) (consistent with conservation of mass).

Furthermore, when the deuteron flux equation is modified by the Einstein relation, the first term now has geometric, material factors, and the ratio of two energies (the applied electric energy organizing the deuterons divided by $k_{\rm B}T$, thermal disorder).

$$k_{\rm E} = \frac{B_{\rm D}qV}{Lk_{\rm B}T} - (k_{\rm G} + k_{\rm F}). \tag{8}$$

The modified deuteron flux equation reveals how competitive gas evolving reactions destroy the desired reactions, and how the ratio of the applied electric field energy to thermal energy ($k_{\rm B}T$) are both decisive in successful LANR experiments.

=>In CF/LANR, despite these unimpeachable equations, the mathematics is surprisingly ignored by most, especially those who fail repeatedly. Also usually ignored is the requisite condition of the loaded lattice, how it loads, its variants and noticing that the desired reactions do not occur at robust levels in their absence.

6.2.4. *CF/LANR requires CAM-driven deuterons and Anderson focusing*

In Pd–D, the key movements on the "road" to successful "cold fusion" (i.e. LANR) begin with the D within the highly loaded Pd. The deuterons are driven by catastrophic desaturation following local temperature increase. This desaturaton, and the rise time to produce by positive feedback, are described by the CAM (catastrophic active media) model. Briefly, after loading (Step 1), there can – under some conditions – occur Step 2 which is the CAM-driven filling of vacancies.

Step 2 - (a reversible step) CAM formation of apo-*He^4 in hyperloaded Vacancies

In summary, the CAM reactions drive the loaded deuterons to the vacancy sites. Equation (9) notes that Takahashi has denoted that clusters of 4 and 6 may also especially enable these desired reactions.

$$\mathrm{nD[D+D+D+D+?]} \Longleftrightarrow \mathrm{4D(H)/TSC\ and\ 6D(H)/OSC\ (Takahashi[149])} \iff \mathrm{apo-{}^4He*} \qquad (9)$$

The Catastrophic Active Medium (CAM) model [135,136] of LANR considers the deuteron solubility in, and the unusual solubility–temperature relationship with, palladium. The complete model involves the saturation of the Pd by D. This is the expected full amount that can be contained therein, and is a function of temperature. The fractional saturation and its interactions with the phonons and the interstitials and vacancies within the palladium better explain how LANR works. Unlike most metals [91,94] characterized by low solubility (∼one deuteron per 10,000 metal atoms), the deuteron solubility in palladium is quite large and decreases with temperature. The CAM model first treats the metallic Pd lattice, into which isotopic fuel is loaded, like a vase for the D (emphore, from *amphora*), and follows the changes in partial saturation of the Pd with D.

Second, the model adds in the fact that the Pd is an active medium capable of rapid desorption of deuterons, with recruitment potential of even more deuterons. This can happen in a paroxysmal and catastrophic way with feedback effects. This has a profound impact on increasing deuteron recruitment, which means the increase of heat produces even more suddenly available deuterons by desorption of D from the Pd (positive feedback [135,136]).

Third, the model reflects that the metallic Pd lattice is heterogeneous, and the model considers *all* types of sites in which the intraelectrode deuterons can reside, including deeper traps supplementing the octahedral and tetrahedral sites. Most importantly, the model documents that the loaded Pd is an active medium capable of rapid deuteron desorption and redistribution (shown in Fig. 7 by τ_{C}), and that there can also be movements into vacancies by Anderson focusing (a solid state effect which focuses D flux into vacancies).

It is the movement of deuterons from throughout the loaded palladium to the active sites that begins the LANR process, and it is augmented by feedback, by phonon-flux coupling, and by the confinement (discussed in the CAM theory from ICCF-4 when the nuclear active site was first introduced). A partial CAM computer model (from ICCF-4) relating the normalized deuteron fugacity, temperature, and the fractional saturation (Fig. 7) shows the relationship of loading, deuterium, and temperature within the cathode. This has been shown to be qualitatively consistent with some experimental observations, as confirmed by Martin Fleischman after ICCF-4.

The model shows that although the deuteron fugacity ($\Theta_{\mathrm{D,Pd}}$) (where fugacity is related to the deuteron pressure [131,133]) rises slightly, thereafter the deuteron saturation curve in Fig. 7 falls rapidly for the loaded palladium. There is a 7-fold decrease in deuteron content from 5 to 50°C. Prior to destruction of the lattice through cracks and dislocations and rupture, this desaturation creates an increase in the intrinsic pressure (fugacity) which follows the intraelectrode deuteron flux from redistribution. Because of the fractional saturation-temperature effect, dynamic inversion of $\Gamma_{\mathrm{D,Pd}}\ (t)$ occurs as $\Theta_{\mathrm{D,Pd}}\ (t)$ and temperature reach crescendo levels.

As a result, after sufficient time, the active site (compartment 2) is suddenly and catastrophically "fed deuterons" from the large vicinal volumes of the crystalline palladium lattice (compartment 1), further increasing the likelihood of additional temperature-incrementing reactions. Eventually, however, the crystal lattice is unable to survive intact, and instead the surface energy normally required to prevent the palladium from escaping, becomes insufficient and the reactants continue to move from their normal sites to accumulate in compartment 2 by the catastrophic reactions and thereby maintain close contact for the desired reactions.

The surface energy required to rupture the palladium prevents the escape of the reactants as they continue to accumulate by the catastrophic reactions and thereby maintain close contact for the desired reactions. Positive feedback comes from the catastrophic behavior secondary to the saturation–temperature relationship. However, when the internal pressures are able to exceed the energy needed to create fresh new surfaces in the palladium, leakage then occurs and the sample becomes, at best, locoregionally inactive.

Simply put, there is injection of deuterons into the vacancies by the sudden catastrophic desaturation of highly loaded Pd. That is followed by a quasiparticle which drives the desired reaction by coupling to the lattice.

6.2.5. *Band states, Bose–Einstein states*

$$\text{apo-}^4\text{He}^* \Longleftrightarrow {}^4\text{He}^*. \tag{10}$$

The lattice enables this reversible reaction through internal conversion (Talbot and Scott Chubb [152–155]). The critical reaction proceeds and is described by either Band States and/or Bose–Einstein states, and other interaction models. It is enabled by the collective excitations of phonons. In addition, it is reasonable to assume that conditions may enable formation of ^{4}He* if and when there is sufficient activation energy (Cravens, Letts, Swartz) [16,23,24,42].

6.2.6. *The Phuson quasiparticle enables coherent collective de-excitation*

The coherent means of excitation of the lattice, the Phuson [161], enables LANR by coherent transfer of energy from ^{4}He* to the lattice. Understanding LANR from this point of view requires closely studying the PHUSON, which is the coherent "particle" of the PHUSON theory. Simply put, the phusons, coherent excitation objects/particles cooperatively transfer energy from the megavoltage energy of the ^{4}He* to the lattice. There results: lattice heating ("excess heat") and de novo ^{4}He. As discussed in the original paper, the PHUSON theory has a mechanism which incorporates the observed products, and the energy levels to all those branches. As a result, it succinctly explains the differences in observed outputs, including the observed "excess heat" as T rises. It also explains the different branches observed near room temperature ("LANR") and at hot fusion temps. The PHUSON theory of LANR has a mechanism which has been, and can be, used to make more reproducible experiments and systems.

Step 3 – (an irreversible step) De-excitation by Phuson to He^4

$$^4\text{He}^*(\text{via PHUSON} - \text{coherent transfer (Swartz)}) \Rightarrow {}^4\text{He}. \tag{11}$$

In this step, there is a critical IRREVERSIBLE ($\sim$20 MeV) transition that is coherent by PHUSON, enabled by phonons, as Hagelstein has described lossy spin bosons [190–194], and (as will shortly be shown) magnons [77,79].

There are many factors that contribute to increase the likelihood of possible fusion: electrical charging of the cathode to a high negative voltage, the deuteron band structure, Bloch-symmetric Bose–Bloch condensates, plasmon exchange, electron screening, and the increased effective mass of the deuterons due to polarons which occur in the crystalline lattice and other dielectrics used.

The coherent de-exciting PHUSON enables the massive energy loss by way of lossy spin bosons processes involving phonons and (as we have shown at ICCF18) magnons. Hagelstein incorporates the optical phonons in his theory. Swartz at ICCF20 has shown these to also include acoustic phonons [69].

The PHUSON cooperatively transfers energy from the megavoltage energy of the ^{4}He* to the lattice in a process which is consistent with conventional physics, and where it appears as "excess heat" [161,162]. The temperature rise occurs as the acoustical and optical phonons become unable to carry off all the momentum and excess energy of the reactions.

Phonon de-excitation modes apparently produce transitional times significant for enabling ^{4}He* to ^{4}He transitions which involving recruitment of sufficient numbers of lattice sites and their associated phonons. After adequate containment time and flux, there is near commensurate amount of excess heat observed in LANR, with the "ash" which is de novo He^4. This process is the unique feature that allows LANR to occur with energy transfer to the lattice.

Specifically, the PHUSON theory explains why there is a relative absence of strong neutron and gamma ray emissions in LANR. The gamma emission branch from the excited state of ^{4}He* is actually spin-forbidden for both hot and cold fusion. However, at higher hot fusion temperatures the restriction is lifted slightly so that some gammas are seen,

and not zero. This spin-forbiddenness of gamma emission is therefore consistent to what is seen for both hot and cold fusion.

The PHUSON theory correctly describes the relative absence of neutrons emissions in LANR. The only nuclear branches available are those whose band gaps are surmountable by the available activation energy (limited by the ambient temperature and incident radiation). The neutron emission branch is more than 1 MeV above the first excited state (^{4}He*). Hot fusion has large activation energies available (it is "hot"). LANR does not. In LANR, given the actual much smaller amount of thermal energy, $k_{\mathrm{B}}T$, available for LANR ($\sim$1/25 eV), absence of adequate activation energy decisively means that that branch is NOT available, as it is for hot fusion. Neutrons are not observed, helium 4 production is in its stead [161,162].

Attention is directed to the fact that the PHUSON theory incorporates the observed products, and the energy levels, which explains the branching ratios based on, and explained by, thermal energies available [161]. It also explains the origin of the excess heat in active LANR systems. The corollary is that the Phuson is a quasiparticle of collective de-excitation observed in high impedance PHUSOR-type CF/LANR systems, and it is quite capable of amplifying incremental power gain significantly.

7. Other Higher Order Systems

Although they are not all related to CF/LANR, some are, and these other higher order systems demonstrate how understanding quasiparticles and collective excitations explain much in physics and material science.

7.1. Quasiparticles of collective excitation – exciton–polaritons, phonon–polaritons, and plasma polaritons

The first example in this higher order categorizations are exciton–polaritons, phonon–polaritons, and plasma–polarons which are quasiparticles of a photon interacting with exciton, phonon, or plasmon, respectively, each arising from collective excitations of a material.

7.2. Quasiparticle of collective excitation – plasmariton – a dressed photon consisting of a plasmon and photon

Another example of a higher order quasiparticle is a plasmariton, which is a photon coupled with both a second optical phonon and a plasmon, a collective excitation.

7.3. Quasiparticle of collective excitation – spinon – quantum spin fluids

Spinons are quasiparticles produced in quantum spin liquids and in rare minerals like Herbertsmithite (Fig. 8) that exhibit magnetic spin liquid states. Herbertsmithite ($ZnCu_3(OH)_6Cl_2$, Mohs hardness $\sim$3.5, 3.76 g/cm^3) has that magnetic anomaly beneath its light-green blue color.

Both it, and its synthetic form, have a Kagome lattice structure, named for the Japanese weaving pattern of repeating triangles, and demonstrate a quantum spin "liquid" in that their domains are neither ferromagnet nor antiferromagnet and instead have "constantly fluctuating scattered orientations". Because of lattice interactions, the magnetic fields are unable to settle into a lowest energy alignment, and must constantly change the direction of their local magnetization. This is confirmed indirectly by neutron scattering.

7.3.1. *Coherent quasi-de-excitation – magnetic Phuson (2nd OOP) enables LANR and is a second pathway for de-excitation*

There is another coherent de-excitation possible in LANR systems, elicited by an applied magnetic field intensity. Previously, magnetic [15,52,97], and radiofrequency electromagnetic [14] effects have been reported in aqueous LANR

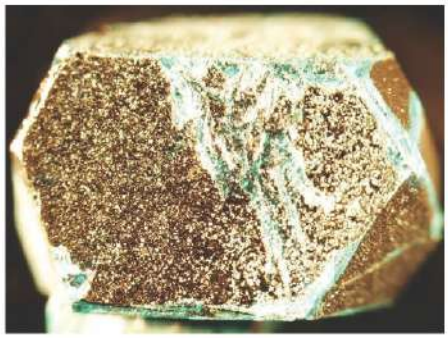

Figure 8. Herbertsmithite containing spinons which demonstrate quantum spin liquids with constantly fluctuating domain magnetic orientation.

systems. In aqueous LANR systems, steady magnetic fields have a small effect which may be inhibitory, especially if perpendicular to the direction of the application of the applied E-field intensity.

Astonishingly, it was discovered that for some magnetic interactions with nanostructured LANR systems [77–79], there is also enhanced improvement of LANR (which occurs at the same time as the applied magnetization and therefore here is called "synchronous"). Also, there is improved LANR excess heat output which also appears later, after the onset of magnetization (since it occurs long after the magnetization when there is no extrinsic magnetic field intensity applied, it is called a "metachronous" effect) and is long-lasting. This was the first evidence of a fractionated high magnetic field intensity producing activation and rejuvenation of nanostructured LANR material, rejuvenating the output to higher levels.

Importantly, as Fig. 9 shows, there results an increase in excess energy gain, and increased incremental power gain, over ordinary LANR. The application of dH/dt created an increase of 4–10 times the peak power gain over conventional LANR with the same system.

The peak power gain of such treated NANOR®s (M-NANOR®s) ranged from 22 to up to ∼80 times input electrical power beyond the ohmic thermal control, as determined by calorimetry.

Pertaining to this paper, there are both synchronous and metachronous impacts after a repeatedly pulsated ("fractionated") magnetic field intensity, both associated with strong evidence of two (2) OOP manifolds [79]. The second OOP is evidence of a second method/means of coherent de-excitation for successful CF/LANR. The first OOP (as described in the literature in the absence of an applied H-field) is enhanced, and in addition the second OOP makes the entire system make even more excess heat, far beyond that expected in the absence of the H-field, making the system quite improved.

The high intensity fractionated system induces a serious secondary E-field as discussed [79], and is even capable of destroying some circuits.

7.3.2. *NANOR®-type CF/LANR components*

Previously, all LANR systems and the NANOR®s had shown a single optimal operating point manifold for excess heat operation, ^{4}He production, and other products. Today, that is no longer accurate, or adequate as an engineering principle, because even after a single treatment to a high intensity fractionated magnetic field, there arise two OOP manifolds. The new one is at higher input electrical currents to the NANOR, and is located to the "right" of the conventional LANR OOP.

Although LANR has a first stage mediated by phonons within the loaded lattice, there is a magnetically coerced

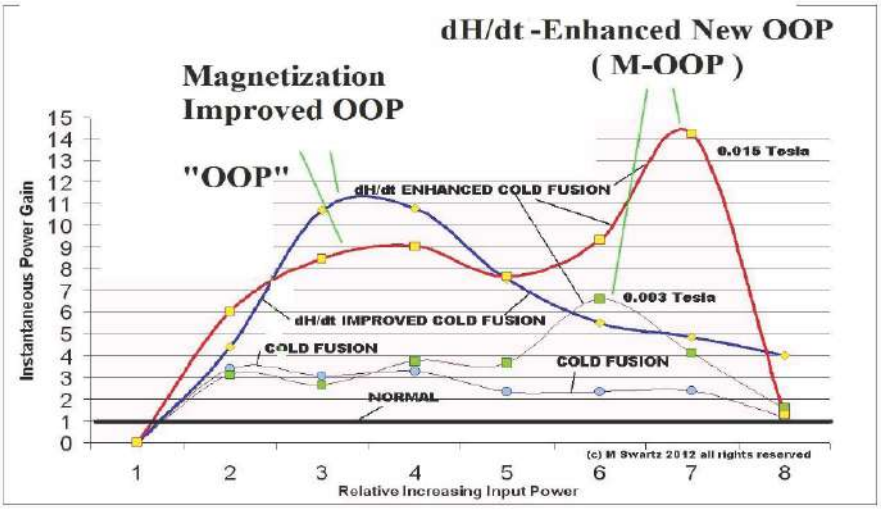

Figure 9. Optical operating point manifolds of LANR, and with and without application of large magnetic field intensities shown against the ohmic control ("normal"). Shown are both synchronous and metachronous results of the applied H-field. A new second ("dH/dt-enhanced) optimal operating point appears ("M-OOP") appears DURING the application of the field, heralding a new LANR pathway.

second stage, which we believe may be mediated by magnons or interactions of phonons with the magnetization field. Magnetization, alignments of magnetic domains, which are observed in such treated NANOR-type components (called "M-NANORs"; [77,79]).

Figure 10 shows curves which plot the electrical input power, at four different input electrical power levels, and the calorimetric responses of both the ohmic control and the preloaded NANOR®-type component. Four complete cycles are shown. The x-axis represents time. The y-axis on the left-hand side represents electrical input power in watts. The y-axis on the right-hand side represents the amount of electrical energy delivered at input, and then released (both the normal electrical dissipation consisting of *VI*, and the excess heat from CF/LANR).

Those curves (on the right hand side axis) represent time integration to determine total energy. They thus rule out energy storage, chemical sources of the induced heat, possible phase changes, and other sources of possible false positives. The units of this axis are in joules.

The figure shows the input, and the calorimetry, of preloaded NANOR along with that for the ohmic thermal control used to calibrate the system. Those calibration pulses, used for accuracy and precision checks of voltages and currents and time, are also shown. The inputs to the thermal ohmic control, followed by the preloaded NANOR®-type component, are shown, as are the calibrated calorimetric outputs for both.

Compare the output for NANOR®-type LANR component to the thermal (ohmic) control. As can be seen, this semiquantitative calorimetry, itself calibrated by thermal waveform reconstruction, was consistent with excess heat being produced only during energy transfer to the NANOR®-type LANR component. Notice that the active preloaded LANR quantum electronic component clearly shows significant improvement in thermal output compared to a standard ohmic control (a carbon composition resistor). The graph, taken after the MIT IAP January 2012 class, is representative of the NANOR-type of LANR technology, and it shows quite clearly demonstrated over unity thermal output power from the demonstration-power-level NANOR-type cold fusion (LANR) component.

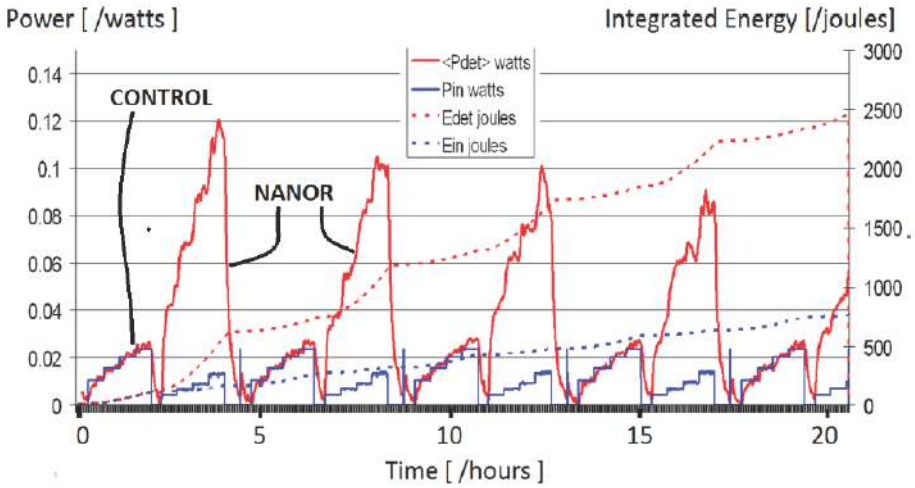

Figure 10. Normal activity of a NANOR®-type component – Before magnetic field. The Electrical Power Input and Thermal Power Output of a two terminal NANOR®-type component Series 6-33 component, showing the calorimetric response at several input powers, for the ohmic control and the component. "Determined" here means measured using ohmic controls and energy balance. Slightly more than four complete cycles are shown. Notice the exponential fall-off characteristic of such components at the peak output. The electrical input power and energy and output thermal power and heat are shown alternatively both from the ohmic control and the NANOR®-type component at several input powers. Note that this component and control was NOT driven in the presence of an applied magnetic field intensity, but only previously had been.

7.3.3. *M-NANOR®-type CF/LANR components*

The proposed Nanoron is a magnetic quasiparticle in magnetized dry preloaded NANOR-type CF/LANR components which produces a second optimal operating point (second pathway) amplifying incremental power gain significantly. Similar to the Spinor, the LANR Nanoron appears to be a potential magnetic quasiparticle picked up initially by the periodic fluctuations in excess heat that had never been seen before. Experimentally, it was also shown later when we were surprised by the two different responses of a NANOR and an M-NANOR. The pre-dH/dt NANOR activity (normal excess heat observed for such active components) is shown in Fig. 10. By contrast, the oscillation of Fig. 11 may reflect the existence of this newly observed magnetic quasiparticle. This appearance is similar to phonons which show their reality through specific heat. Here, this quasiparticle shows its existence through changes in sample activity (like Herbertsmithite does with induced magnetization). Figure 11 shows the input power and output heat flow normalized to input electrical power of a self-contained LANR quantum electronic component AFTER it was magnetically treated [79], and magnetized [77]. Twelve complete cycles are shown. Note the absence of an exponential or linear fall-off of peak activity. Notice that the peak power gain oscillates, never seen in previous unmagnetized NANOR®-type components. This experimental run of a M-NANOR®-type component was made several hours after a single application sequence of the fractionated magnetic field was delivered. There was no additional H-field applied for this figure. The energy curves are very light, but are there as dotted lines.

There is enhanced improvement of LANR (which is synchronous), and improved LANR which is metachronous and longer-lasting. Notice the exponential falloff of the peak incremental excess power gain in Fig. 10 compared to the unusual behavior in Fig. 11. Specifically, contrast the previous slowly falling response to the more bizarre, not seen before, "oscillation" which occurred after the component was exposed to a dH/dt field) while in the active mode with an applied E field to activate it (Fig. 11).

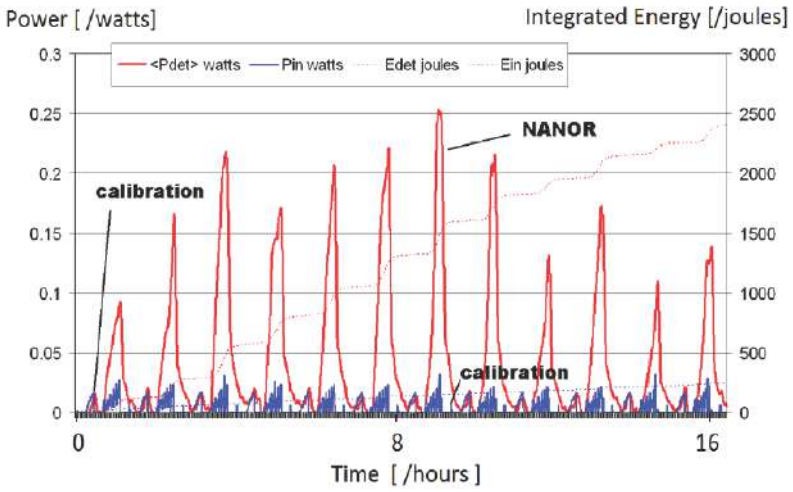

Figure 11. Nanoron – quasiparticle observed as magnetization impact on LANR Activity. Input power and output heat flow normalized to input electrical power of a self-contained LANR quantum electronic component at 124 V peak input voltage.

Specifically, it is important to remember that in Fig. 11, there was no additional H-field applied during the measurements, although a very small, second order H-field is induced in both the components shown in Figs. 10 and 11, by the applied E-field used to activate them.

Similar to the spinon described above, this oscillation of power gain in Fig. 11 may be secondary to a quasiparticle of a coherent de-excitation. We are presently examining an analysis of the force density and homogeneous oscillation frequency using the Maxwell stress tensor [77].

8. Conclusion

Quasiparticles, collective excitations and their higher order quasiparticles of coherent excitations, open up new understanding into material science and engineering. Consider that this brief introduction has not even considered rotons of superfluids, Weyl fermions (Types I and II), dropletons, anyons, and the Bogoliubov quasiparticle from a broken Cooper pair charged electron and hole. There are many more types of quasiparticles, collective excitation and their higher-order particles. They will be examined more, and others sought, in the coming years.

As discussed, from an electrical engineering point of view, quasiparticles, collective excitations and their higher order coherent excitations, discussed here, are also highly relevant to LANR, and in multiple material ways.

Specifically, the L,D-defects, CAM and PHUSON models suggest that quasiparticles and collective excitation have a clear fundamental role in successful CF/LANR. They enable loading of Pd with D, and in that loaded Pd they enable the volumetric redistribution of loaded deuterons followed by high-energy nuclear states returning to their ground state by internal conversion using plasmons, phonons, and sometimes magnons. In summary, these quasiparticles and coherent de-excitations enable successful CF/LANR.

Acknowledgments

The author thanks Gayle Verner and David Nagel for their meticulous help and suggestions for this manuscript. The author acknowledges and thanks Gayle Verner for her very helpful editorial support. This effort was supported by JET

Energy Inc. and the New Energy Foundation. NANOR® and PHUSOR® are registered trademarks of JET Energy, Incorporated. NANOR®-technology, and PHUSOR®-technology are protected by U.S. Patents D596724, D413659 and several other patents pending.

References

[1] A. Von Hippel (Ed.), *Dielectric Materials and Applications*, MIT Press, Cambridge, 1954.

[2] A. Von Hippel (Ed.), *The Molecular Designing of Materials and Devices*, MIT Press, Cambridge, 1965.

[3] C. Kittel, *Introduction to Solid State Physics*, 8th Edition, ISBN:978-0-471-41526-88th Edition (2004).

[4] Neil W. Ashcroft and N. David Mermin, *Solid State Physics*, ISBN-13: 978-0030839931, Brooks Cole, 1976.

[5] J.R. Melcher, *Continuum Electromechanics*, MIT Press, Cambridge, 1981.

[6] M.R. Swartz, Survey of the observed excess energy and emissions in lattice assisted nuclear reactions, *J. Scientific Exploration* **23** (4) (2009) 419–436.

[7] M. Miles, R.A. Hollins, B.F.Bush, J.J. Lagowski and R.E. Miles, Correlation of excess power and helium production during D_2O and H_2O electrolysis using palladium cathodes, *J. Electroanal. Chem.* **346** (1993) 99–117; M.H. Miles Trans.and B.F. Bush, Heat and helium measurements in deuterated palladium, *Trans. Fusion Technol.* **26** (1994) 156–159.

[8] M. Srinivasan et al., Tritium and excess heat generation during electrolysis of aqueous solutions of alkali salts with nickel cathode, *Frontiers of Cold Fusion*, H. Ikegami (Ed.), *Proc. Third Int. Conf. on Cold Fusion*, October 21–25, 1992, Universal Academy Press, Tokyo 123–138.

[9] F.G. Will, K. Cedzynska and D.C. Linton, Tritium generation in palladium cathodes with high deuterium loading, *Trans. Fusion Technol*. **26** (1994) 209–213.

[10] F.G. Will, Reproducible tritium generation in electrochemical cells employing palladium cathodes with high deuterium loading, *J. Electroanal. Chem***. 360** (1993) 161–176.

[11] L.C. Case, Catalytic fusion of deuterium into helium-4, in *The Seventh Int. Conf. on Cold Fusion*, Vancouver, Canada, ENECO Inc., Salt Lake City, UT, 1998.

[12] M.R. Swartz, C. Haldemann, A. Weinberg and B. Ahern, Possible deuterium loss during excess heat from ordinary water-carbonate electrolyte using nickel, in preparation.

[13] M.R. Swartz, Excess power gain using high impedance and codepositional LANR devices monitored by calorimetry, heat flow and paired stirling engines, *Proc. ICCF14* 1 (2008) D.J. Nagel and M.E. Melich (Eds.), ISBN: 978-0-578-06694-3, **123** (2010) 123; www.iscmns.org/iccf14/PICCF14a.pdf.

[14] J. OM. Bockris, R. Sundaresan, D. Letts and Z.S. Minevski, Triggering and structural changes in cold fusion electrodes, *Proc. ICCF4*, Maui, Hawaii, 1993.

[15] D. Cravens, Factors affecting success rate of heat generation in CF cells, *Proc. ICCF-4*.

[16] D. Cravens, Letts and P. Hagelstein, Progress on two-laser experiments, *Proc. ICCF15*, 2009, http://lenr-canr.org/acrobat/Hagelsteinprogresson.pdf).

[17] I. Dardik, H. Branover, A. El-Boher, D. Gazit, E. Golbreich, E. Greenspan, A. Kapusta, B. Khachatorov, V. Krakov, S. Lesin, B. Michailovitch, G. Shani and T. Zilov, Intensification of low energy nuclear reactions using superwave excitation, *Proc. 10th Int. Conf. on Cold Fusion,* 2003.

[18] J. Dash and S. Miguet, Microanalysis of Pd cathodes after electrolysis in aqueous acids, *J. New Energy* **1**(1) (1996) 23.

[19] M. Fleischmann and S. Pons, Calorimetry of the Pd–D_2O system: from simplicity via complications to simplicity, *Phys. Lett*. A **176** (1993) 118–129.

[20] M. Fleischmann and S. Pons, Electrochemically induced nuclear fusion of deuterium, *J. Electroanal. Chem.* **261** (erratum, **263**, 187) (1989) 301–308.

[21] M. Fleischmann and S. Pons, Some comments on the paper analysis of experiments on calorimetry of LiOD/D_2O electrochemical cells, R.H.Wilson et al., *J. Electroanal. Chem*. 332 (1992) 1*, *J. Electroanal. Chem.* **332** (1992) 33–53.

[22] M. Fleischmann, S. Pons, M. Anderson, L.J. Li and M. Hawkins, Calorimetry of the palladium–deuterium–heavy water system, *Electroanal. Chem*. **287** (1990) 293.

[23] D. Letts and D. Cravens, Laser stimulation of deuterated palladium: past and present, *Proc. 10th Int. Conf. on Cold Fusion*, 2003.

[24] D. Letts and P.L. Hagelstein, Stimulation of optical phonons in deuterated palladium, in *ICCF-14 Int. Conf. on Condensed Matter Nucl. Sci.,* 2008, Washington, DC; D. Letts, D. Cravens and P.L. Hagelstein, Thermal *Changes in Palladium Deuteride Induced by Laser Beat Frequencies, in Low-Energy Nuclear Reactions*, Sourcebook, J. Marwan and S. Krivit (Eds.), 2008, Oxford University Press, Oxford, D. Letts and D. Cravens, Laser stimulation of deuterated palladium: past and present, in *Tenth Int. Conf. on Cold Fusion*, 2003, Cambridge, MA.

[25] X.Z. Li et al., The precursor of cold fusion phenomenon in deuterium/solid systems. in anomalous nuclear effects in deuterium/solid systems, *AIP Conf. Proc.* 228, 1990, Brigham Young Univ. Provo, UT, American Institute of Physics, New York.

[26] F.J. Mayer, J. S. King and J.R. Reitz, Nuclear fusion from crack-generated particle acceleration, *J. Fusion Energy* **9** (1990) 269–271, F.J. Mayer and J.R. Reitz, Nuclear energy release in metals, *Fusion Technol*. **19** (1991) 552.

[27] McKubre, F. Tanzella, P. Hagelstein, K. Mullican and M. Trevithick, The need for triggering in cold fusion reactions, *Proc. 10th Int. Conf. on Cold Fusion,* 2003.

[28] G.H. Miley, G. Narne and T. Woo, Use of combined NAA and SIMS analyses for impurity level isotope detection, *J. Radioanal. Nucl. Chem.* **263**(3) (2005) 691–696.

[29] G.H. Miley and J. Shrestha, Transmutation reactions and associated LENR effects in solids, in *Low-Energy Nuclear Reactions*, Sourcebook, J. Marwan and S. Krivit (Eds.), 2008, Oxford University Press, Oxford.

[30] Mosier-Boss and S. Szpak, The Pd/nH system: transport processes and development of thermal instabilities, *Il Nuovo Cimento* **112A** (1999) 577–585.

[31] S. Pons and M. Fleischman, Heat after death, *Proc. ICCF-4*, Maui, EPRI TR104188-V2 2, 8-1 (1994); *Trans. Fusion Technol*. **26**, 4T art 2 (1994) 87.

[32] M.R. Swartz, C. Haldemann, A. Weinberg and B. Ahern, Possible deuterium loss during CF/LANR using nickel ordinary water, in preparation.

[33] M.R. Swartz, Consistency of the biphasic nature of excess enthalpy in solid state anomalous phenomena with the quasi-1-dimensional model of isotope loading into a material, *Fusion Technol*. **31** (1997) 63–74.

[34] M.R. Swartz, Improved electrolytic reactor performance using π-notch system operation and gold anodes, *Trans. American Nuclear Association*, Nashville, Tenn Meeting (ISSN:0003-018X publisher LaGrange, Ill) **78** (1998) 84–85.

[35] M.R. Swartz, Optimal operating point characteristics of nickel light water experiments, *Proc. ICCF-7* (1998).

[36] M.R. Swartz, Optimal operating points in active, loaded palladium linked to three distinct physical regions, in *Fourteenth Int. Conf. on Cold Fusion*, 2008, Washington, DC, p. 639.

[37] M.R. Swartz, Spatial and temporal resolution of three sites characterizing lattice-assisted nuclear reactions, APS 2008; M. Swartz, *Colloquium on LANR in Deuterated Metals Colloquium on LANR at MIT,* August 2007.

[38] M.R. Swartz, The impact of heavy water (D_2O) on nickel-light water cold fusion systems, *Proc. 9th Int. Conf. on Cold Fusion (Condensed Matter Nuclear Science)*, Beijing, China, Xing Z. Li, May (2002) 335–342.

[39] M.R. Swartz and G. Verner, Can a Pd/D_2O/Pt device be made portable to demonstrate the optimal operating point, *ICCF-10* (Cambridge, MA), 2003, *Condensed Matter Nuclear Science*, Peter L. Hagelstein, Scott and R. Chubb (Eds.), World Scientific, NJ, ISBN 981-256-564-6 (2006) 45–54.

[40] M.R. Swartz and G. Verner, Dual ohmic controls improve understanding of "Heat after Death", *Trans. Amer. Nucl. Soc.* **93** (2005) 891–892, ISSN:0003-018X.

[41] M.R. Swartz and G. Verner, Excess heat from low electrical conductivity heavy water spiral-wound Pd/D_2O/Pt and Pd/D_2O–$PdCl_2$/Pt devices, *Condensed Matter Nuclear Science, Proc. ICCF-10*, Peter L. Hagelstein, Scott and R. Chubb (Eds.), World Scientific, NJ, 2006, pp. 29–44; 45–54, ISBN 981-256-564-6.

[42] M.R. Swartz and G. Verner hotoinduced excess heat from laser-irradiated electrically-polarized palladium cathodes in D_2O, *Condensed Matter Nuclear Science, Proc. ICCF-10* Peter L. Hagelstein, Scott and R. Chubb (Eds.), World Scientific, NJ, 2006, pp. 213–226, ISBN 981-256-564-6.

[43] M.R. Swartz and G. Verner, Two site of cold fusion reactions viewed by their evanescent tardive thermal power, Abstract *ICCF-11* (2004); M. Swartz, Kinetics and Lumped Parameter Model of Excess Tardive Thermal Power, M. Swartz, *APS*, 2005.

[44] M.R. Swartz, Spatial and temporal resolution of three sites characterizing lattice-assisted nuclear reactions, *APS* 2008; M. Swartz, *Colloquium on LANR in Deuterated Metals Colloquium on LANR at MIT*, August 2007.

[45] M.R. Swartz, Gayle Verner and Alan Weinberg ossible non-thermal near-IR emission linked with excess power gain in high impedance and codeposition Phusor-LANR devices, in *Fourteenth Int. Conf. on Cold Fusion*, 2008, Washington, DC.
[46] M.R. Swartz, *Trans. Amer. Nucl. Assoc.* **78** (1998) 84–85.
[47] M.R. Swartz, G. Verner and Alan Weinberg, Non-thermal near-IR emission from high impedance and codeposition LANR devices, *Proc. ICCF14* **1** (2010) 343ISBN: 978-0-578-06694-3.
[48] V. Violante, E. Castagna, C. Sibilia, S. Paoloni and F. Sarto, Analysis of mi-hydride thin film after surface plasmons generation by laser technique, *Proc. 10th Int. Conf. on Cold Fusion* (2003).
[49] S. Szpak .A. Mosier-Boss, R.D. Boss and J.J. Smith, On the behavior of the Pd/D system: evidence for tritium production, *Fusion Technol.* **33** (1998) 38–51.
[50] P.A. Mosier-Boss, S. Szpak, F.E. Gordon and L.P.G. Forsley, Use of CR-39 in Pd/D co-deposition experiments, *Euro. P Phys. J.-Appl. Phys.* **40** (2007) 293–303.
[51] P.A. Mosier-Boss, L. P. Forsley, F.E. Gordon, D. Letts, D. Cravens, M. H. Miles, M. Swartz, J. Dash, F. Tanzella . Hagelstein, M. McKubre and J. Bao, Condensed matter nuclear reaction products observed in Pd/D codeposition experiments, *Current Sci.* **108** (4) (2015) 656. http://www.currentscience.ac.in/Volumes/108/04/0656.pdf.
[52] S. Szpak .A. Mosier-Boss and F.E. Gordon, Further evidence of nuclear reactions in the Pd/D lattice: emission of charged particles, *Naturwissenschaften* **94** (2007) 511–514.
[53] S. Szpak .A. Mosier-Boss and J.J. Smith, On the behavior of the cathodically polarized Pd/D system: search for emanating radiation *Phys. Letts*. A **210** (1996) 382–390.
[54] S. Szpak, .A. Mosier-Boss and F. Gordon, Further evidence of nuclear reactions in the Pd lattice: emission of charged particles, *Naturwissenschaften* DOI 10.1007 (2007).
[55] M.R. Swartz, Codeposition of palladium and deuterium, *Fusion Technol.* **32** (1997) 126–130.
[56] S. Szpak and P.A. Mosier-Boss, On the behavior of the cathodically polarized Pd/D system: a response to vigiers comments *Phys. Letts*. A **221** (1996) 141–143.
[57] S. Szpak, A. Mosier-Boss and J.J. Smith, Deuterium uptake during Pd–D codeposition, *J. Electroanal. Chem.* **379** (1994) 121–127.
[58] S. Szpak, A. Mosier-Boss and J.J. Smith, On the behavior of Pd deposited in the presence of evolving deuterium, *J. Electroanal. Chem*. **302** (1991) 255–260.
[59] S. Szpak, A. Mosier-Boss, C. Young and F.E. Gordon, Evidence of nuclear reactions in the Pd Lattice, *Naturwissenschaften* **92** (2005) 394–397.
[60] S. Szpak, A. Mosier-Boss, M.H. Miles and M. Fleischmann, Thermal behavior of polarized Pd/D electrodes prepared by co-deposition, *Thermochim. Acta* **410** (2004) 101–107.
[61] S. Szpak, A. Mosier-Boss, S.R. Scharber and J.J. Smith, Charging of the Pd/nH system: role of the interphase, *J. Electroanal. Chem*. **337** (1992) 147–163.
[62] S. Szpak, A. Mosier-Boss, S.R. Scharber and J.J. Smith, Cyclic voltammetry of Pd+D codeposition, *J. Electroanal. Chem*. **380** (1995) 1–6.
[63] S. Szpak, A Mosier-Boss, C. Young and F.E. Gordon, The effect of an external electric field on surface morphology of co-deposited Pd/D films, *J. Electroanal. Chem.* **580** (2005) 284–290.
[64] S. Szpak, C.J. Gabriel, J.J. Smitch and R.J. Nowak, Electrochemical charging of Pd rods, *J. Electroanal. Chem.* **309** (1991) 273–292.
[65] Y. Arata and Y.C. Zhang, Observation of anomalous heat release and helium-4 production from highly deuterated fine particles, *Jpn. J. Appl. Phys.* Part 2, **38** (1999) L774.
[66] M.R. Swartz, Incremental high energy emission from a ZrO_2–PdD nanostructured quantum electronic component CF/LANR, *J. Condensed Matter Nucl. Sci.* **15** (2015) 92. www.iscmns.org/CMNS/JCMNS-Vol15.pdf.
[67] M.R. Swartz, G. Verner, J. Tolleson, L. Wright, R. Goldbaum, Mosier-Boss and P.L. Hagelstein, Imaging of an active NANOR®-type LANR component using CR-39, *J. Condensed Matter Nucl. Sci*. **15** (2015) 81. www.iscmns.org/CMNS/JCMNS-Vol15.pdf.
[68] M.R. Swartz, Optical detection of phonon gain distinguishes an active cold fusion/LANR component, *J. Condensed Matter Nucl. Sci*. **20** (2016) 29–53.
[69] M.R. Swartz and P. Hagelstein, Increased PdD anti-Stokes peaks are correlated with excess heat mode, *Proc. ICCF-20,*

submitted for publication.
[70] Y. Arata and Y.C. Zhang, Anomalous production of gaseous ^{4}He at the inside of DS-cathode during D_2-electrolysis, *Proc. Jpn. Acad. Ser. B* **75** (1999) 281.
[71] Y. Arata and Y. Zhang, The establishment of solid nuclear fusion reactor*, J. High Temp. Soc.* **34**(2) (2008) 85.
[72] M.R. Swartz, P.L. Hagelstein and G. Verner, Impact of electrical avalanche through a ZrO_2-NiD nanostructured CF/LANR component on its incremental excess power gain, *ICCF-19*, *J. Condensed Matter Nucl. Sci*. (2016) 19.
[73] M.R. Swartz, G. Verner, J. Tolleson and P. Hagelstein, Dry reloaded NANOR®-type CF/LANR components, *Current Sci.* **108** (4) (2015) 595. http://www.currentscience.ac.in/Volumes/108/04/0595.pdf.
[74] M.R. Swartz and P.L. Hagelstein, Demonstration of energy gain from a preloaded ZrO_2–PdD nanostructured CF/LANR quantum electronic device at MIT, *J. Condensed Matter Nucl. Sci*. **13** (2014) 516. www.iscmns.org/CMNS/JCMNS-Vol13.pdf.
[75] M.R. Swartz, P.L. Hagelstein and G. Verner, Impact of electrical avalanche through a ZrO_2–NiD nanostructured CF/LANR component on its incremental excess power gain, *ICCF-19*, Padua, Italy, April 16, 2015.
[76] M.R. Swartz and G. Verner, Energy gain from preloaded ZrO_2–PdNi–D nanostructured CF/LANR quantum electronic components, *J. Condensed Matter Nucl. Sci.* **13** (2014) 528. www.iscmns.org/CMNS/JCMNS-Vol13.pdf.
[77] M.R. Swartz, Oscillating excess power gain and coerced magnetic domains in M-NANOR-type CF/LANR components, *J. Condensed Matter Nucl. Sci.* **22** (2017) 38–46.
[78] M.R. Swartz, Impact of an applied magnetic field on a high impedance dual anode LANR device, *J. Condensed Matter Nucl. Sci.* **4** (2011) 93; 239th American Chemical Society National Meeting and Exposition in San Francisco (2011). www.iscmns.org/CMNS/JCMNS-Vol4.pdf.
[79] M.R. Swartz, G. Verner, J. Tolleson, L. Wright, R. Goldbaum and P. Hagelstein, Amplification and restoration of energy gain using fractionated magnetic fields on ZrO_2–PdD nanostructured components, *J. Condensed Matter Nucl. Sci*. **15** (2015) 66. www.iscmns.org/CMNS/JCMNS-Vol15.pdf.
[80] D. Cravens, M. Swartz and B. Ahern, Condensed matter nuclear reactions with metal particles in gases, *Current Sci*. **108** (4) (2015) 582. http://www.currentscience.ac.in/Volumes/108/04/0582.pdf.
[81] Y. Iwamura, M. Sakano and T. Itoh, Elemental analysis of Pd complexes: effects of D_2 gas permeation, *Jpn. J. Appl. Phys.* A **41 (**2002) 4642.
[82] Y. Iwamura, T. Itoh, N. Yamazaki, J. Kasagi, Y. Terada, T. Ishikawa, D. Sekiba, H. Yonemura and K. Fukutani, Observation of surface distribution of products by X-ray fluorescence spectrometry during D_2 gas permeation through Pd complexes, in *The 12th Int. Conf. on Condensed Matter Nucl. Sci.,* 2005. Yokohama, Japan.
[83] R. Stringham, Cavitation and fusion, *Tenth Int. Conf. on Cold Fusion*, 2003, Cambridge, MA.
[84] R. George (personal communication); C. Platt, What if cold fusion is real? *Wired Magazine*, Nov. 1, 1998, https://www.wired.com/1998/11/coldfusion/
[85] D. Nagel, *ICCF13*, Sochi, Russia owners, Materials and Radiations from Low Energy Nuclear Reactions on Surfaces, 2007.
[86] M.R. Swartz, Noise measurement in cold fusion systems, *J. New Energy* **2**(2) (1997) 56–61.
[87] J.C. Dickinson, L.C. Jensen, S.C. Langford and R.R. Ryan, Fracto-emission from deuterated titanium: supporting evidence for a fracto-fusion mechanism, *J. Mater. Res.* **5** (1990) 109.
[88] M.R. Swartz, Atterns of failure in cold fusion experiments, *Proc. 33rd Intersociety Engineering Conf. on Energy Conversion*, IECEC-98-I229, CO, Aug. 1998.
[89] M.R. Swartz, Atterns of success in research involving low-energy nuclear reactions, *Infinite Energy* **31** (2000) 46–48.
[90] F.A. Cotton and G. Wilkinson, *Advanced Inorganic Chemistry*, Interscience, NY, 1972.
[91] C.A. Hampel, *Rare Metal Handbook*, Reinhold, NY, 1954.
[92] E. Orowan, Surface energy and surface tension in solids and liquids, *Proc. Roy. Soc. Lond.* A **316** (1970) 173–191.
[93] R.W. Bussard, Virtual-state internal nuclear fusion in metal lattices, *Fusion Technol.* **16** (1989) 231–236.
[94] C.J. Smithell, *Metals Reference Book*, Btterworths, 1949.
[95] D.R. Rolison and P.P. Trzaskoma, Morphological differences between hydrogen-loaded and deuterium-loaded palladium as observed by SEM, *J. Electroanal. Chem*. **287** (1990) 287.
[96] C.R.A. Catlow, Atomic transport in heavily defective solids, *Phill Magazine* A **64** (5) (1991) 1011–1024.
[97] B.M. Klein and R.E. Cohen, Anharmonicity and the inverse isotope effect in the palladium–hydrogen system, *Phys, Rev*. B

45 (21) (1992) 405.
[98] D.A. Papaconstantopoulos, B.M. Klein, E.N. Economou and L.L Boyer, Band structure and superconductivity of PdDx and PdHx hysical Review, **17**, 1 (1977) 141–150.
[99] A. Pusch, W. Fenzl and J. Peisll, Hydrogen in niobium under pressure, *J. Less-Common Metals* **172–174** (1991) 709–717.
[100] H.R. Schober and A.M. Stoneham, Diffusion of hydrogen in transition metals, *J. Less-Common Metals*, **172–174** (1991) 538–547.
[101] H. Teichler, Theory of hydrogen hopping dynamics including hydrogen-lattice correlations, *J. Less-Common Metals* **172–174** (1991) 548–556.
[102] P. Vargas, L. Miranda, L. Rodriguez, M. Lagos and J. Rogan, Quantum diffusion in transition metals, *J. Less-Common Metals* **172–174** (1991) 557–571.
[103] E. Wicke and H. Brodowsky, *Hydrogen in Palladium and Palladium Alloys, Hydrogen in Metals II,* G. Alefield and J. Volkl (Eds.), Springer, Berlin, 1978.
[104] H. Zuchner and T. Rauf, Electrochemical measurements of hydrogen diffusion in intermetallic compound LaNi5*, J. Less-Common Metals* **172–174** (1991) 611–617.
[105] R.V. Bucur, Interaction of Hydrogen with the Microstructure in Pd and Pd77Ag23, Cumo Italy, 1991, p. 28.
[106] G.L. Powell, J.R. Kirkpatrick and J.W. Conant, Surface effects in the reaction of H and D with Pd-macroscopic manifestations, *J. Less-Common Metals* **172–174** (1991) 867–872.
[107] K.H. Johnson, Jahn–Teller, Symmetry breaking and hydrogen energy in g-PdD cold fusion as storage of the latent heat of water, *Cold Fusion Source Book*, ibid. **75** (1994).
[108] L. DeChiaro, L. Forsley and P.A. Mosier-Boss, Strained layer ferromagnetism in transition metals and its impact upon low energy nuclear reactions, *J. Condensed Matter Nucl. Sci*. 2015.
[109] J.M. Ok, Y.J. Jo, K. Kim,T. Shishidou, E.S. Choi, H.J. Noh, T. Oguchi, B.I. Min and J.S. Kim, Quantum oscillations of the metallic triangular-lattice antiferromagnet $PdCrO_2$, *Phys Rev. Lett*. **111**(17) 176405. Epub Oct 25 (2013).
[110] D.L.R. Santos, P. Venezuela, R.B. Muniz and A.T. Costa, Spin pumping and interlayer exchange coupling through palladium, *Phys. Rev*. **88** B (2013) 054423.
[111] S. Shimizu, K.S. Sunao, A. Takahashi, T. Hatano, M. Kawasaki, Y. Tokura and Y. Iwasa, Electrically tunable anomalous hall effect in Pt thin films, *Phys. Rev. Lett*. **111** (2013) 216803.
[112] Y. Sun, J.D. Burton and E.Y. Tsymbal, Electrically driven magnetism on a Pd thin film, *Phys. Rev*. B **81** (2010) 064413.
[113] S. Shimizu, K.S. Takahashi, T. Hatano, M. Kawasaki, Y. Tokura and Y. Iwasa, Electrically tunable anomalous Hall effect in Pt thin films, *Phys. Rev. Lett*. **111** (2013) 216803.
[114] M. Apicella, E. Castagna, L. Capobianco, L. DAulerio, G. Mazzitelli, F. Sarto, A. Rosada, E. Santoro, V. Violante, M. McKubre and F. Tanzella, Some recent results at ENEA, *The 12th Int. Conf. on Condensed Matter Nucl. Sci.*, 2005.
[115] M. Swartz, Dances with protons-ferroelectric inscriptions in water/ice relevant to cold fusion and some energy systems, *Infinite Energy* **44** (2002).
[116] N. Bjerrum, K. Danske, V. Selskab, *Met.-Fys. Medd*. **27** (1951) 1.
[117] P. Bridgman, *The Physics of High Pressure*, C. Bell, London, 1949.
[118] M. Eigen and L. De Maeyer, *Proc. Roy. Soc*. (London) **247 A** (1958) 505.
[119] M. Eigen, L. De Maeyer and H.-Ch. Spatz, *Ber. Bunsen Ges. Phys. Chem*. **68** (l964) 19.
[120] D. Eisenberg and W. Kauzmann, *The Structure and Properties of Water*, Oxford University Press, New York, 1969.
[121] N. Fletcher, *The Chemical Physics of Ice*, Cambridge University Press, New York, 1970.
[122] F. Franks, *Water, a Matrix of Life*, Royal Society of Chemistry, Cambridge, UK.
[123] B. Kamb, *Ice Polymorphism and the Structure of Water, in Structural Chemistry and Molecular Biology*, A. Rich and N. Davidson (Eds.), a volume dedicated to Linus Pauling by his students, colleagues and friends, W. H.Freeman, San Francisco, 1968, pp. 507–512. Also Structural studies on the high-pressure forms of ice, *Trans. Amer. Cryst. Assoc*. **5** (1969) 61.
[124] A. von Hippel, *Dielectric Materials and Applications*, MIT Press, Cambridge, USA, 1954.
[125] A. von Hippel and E.F. Farrell, *Mat. Res. Bull*. **8** (1973) 127.
[126] A. von Hippel, *Molecular Mechanisms of Conduction and Polarization in Water Vapor, Liquid Water and Ice*, LIR MIT, Cambridge, USA, 1972–1973.
[127] A. von Hippel, J. *Chem. Phys*. **54** (1971) 145.

[128] A. von Hippel, D.B. Knoll and W.B. Westphal, Transfer of protons through pure ice 1_h single crystals, *J. Chem. Phys*. **54** (1971) 134, 145.
[129] M.R. Swartz P.L. Hagelstein, G. Verner and K. Wright, Transient vacancy phase states in palladium following high dose rate electron beam irradiation, *J. New Energy* (2003).
[130] N. Takanol, T.Kai, K.Shiiki and F.Terasakil, Effect of copious vacancies on magnetism of Pd, *Solid State Commun.* **97** (2) (1996) 153–156.
[131] J. O′M Bockris and A. Reddy, *Modern Electrochemistry*, Plenum Press, 1970.
[132] M. Swartz, Kinetics and lumped parameter model of excess tardive thermal power, *APS* (2005).
[133] H.H. Uhlig, *Corrosion and Corrosion Control*, Wiley, New York, 1971.
[134] H. Ezaki, M. Morinaga and S. Watanabe, Hydrogen overpotential for transition metals and alloys and its interpretation using an electronic model, *Electrochimica Acta* **38** (1993) 557–564.
[135] M.R. Swartz, Hydrogen redistribution by catastrophic desorption in select transition metals, *J. New Energy* **1** (4) (1997) 26–33.
[136] M.R. Swartz, Catastrophic active medium hypothesis of cold fusion, Vol**. 4**, *Proc. Fourth Int. Conf. on Cold Fusion*, ibid. (1994).
[137] M.R. Swartz, Control of low energy nuclear systems through loading and optimal operating points, *ANS/ 2000 Int. Winter Meeting*, Nov. 12–17, 2000, Washington, DC, 2000.
[138] M.R. Swartz, Generality of optimal operating point behavior in low energy nuclear systems, *J. New Energy* **4**(2) (1999) 218–228.
[139] M.R. Swartz, Generalized isotopic fuel loading equations, *Cold fusion Source Book*, *Int. Symposium on Cold Fusion and Advanced Energy systems*, Hal Fox (Ed.), Minsk, Belarus, May 1994.
[140] M.R. Swartz, Isotopic fuel loading coupled to reactions at an electrode, *Fusion Technol.* **26** (4T) (1994) 74–77.
[141] M.R. Swartz, Quasi-one-dimensional model of electrochemical loading of isotopic fuel into a metal, *Fusion Technol*. **22** (2) (1992) 296–300.
[142] R.W. Bass and M. Swartz, Empirical system identification (ESID) and optimal control of lattice assisted nuclear reaction (LANR) devices, *ICCF14*, August 14, 2008.
[143] M.R. Swartz and L. Forsley. Analysis of superwave-as-transitory-OOP-peak hypothesis, in *ICCF-14 Int. Conf. on Condensed Matter Nuclear Science*, 2008, Washington, DC.
[144] M. Rabinowitz, Y. Kim, V. Chechin and V. Tsarev, Opposition and support for cold fusion. in *Fourth Int. Conf. on Cold Fusion*, Lahaina, Maui: Electric Power Research Institute 3412 Hillview Ave. alo Alto, CA 94304 (1993) 15–1.
[145] M. Rabinowitz and D.H. Worledge, An analysis of cold and lukewarm fusion, *Fusion Technol.* **17** (1990) 344.
[146] M. Rabinowitz, Y.E.Kim, V.A.Chechin and V.A.Tsarev, Opposition and support for 146 cold fusion, 15–1 to 15–12, Vol. 2, *Proc. Fourth Int. Conf. on Cold Fusion*, sponsored by EPRI and the Office of Naval Research, December (1994).
[147] J. Schwinger, Cold fusion: a hypothesis, *Zeitschrift f. Natur*. A **45** (1990) 756.
[148] R.A. Rice, G.S. Chulick and Y.E. Kim, Effect of velocity distribution and electron screening on cold fusion, *Proc. ACCF1*, Salt Lake City, 1990, p. 185.
[149] A. Takahashi and N. Yabuuchi, Study on 4D/TSC condensation motion by non-linear langevin equation, in low-energy nuclear reactions, *Sourcebook*, J. Marwan and S. Krivit (Eds.), 2008, Oxford University Press, Oxford. A. Takahashi, Dynamic mechanism of TSC ##. in *ICCF-14 Int. Conf. on Condensed Matter Nuclear Science*, 2008, Washington, DC.
[150] H. Hora, J.C. Kelly, J.U. Patel, Mark A. Prelas, G.H. Miley and J.W. Tompkins, Screening in cold fusion derived from D–D reactions, *Phys. Lett*. A 175 (1993) 138–143.
[151] G. Preparata, *Fusion Technol.* **20** (1991) 82.
[152] T.A. Chubb and S.R. Chubb, Ion band states: what they are and how they affect cold fusion, *Cold Fusion Source Book*, ibid., *75* (1994).
[153] S.R. Chubb and T.A. Chubb, The role of hydrogen ion band states in cold fusion, *Trans. Fusion Technol.* **26**(4T) (1994) 414.
[154] S.R. Chubb and T.A. Chubb. An explanation of cold fusion and cold fusion by-products, based on lattice induced nuclear chemistry. in *Second Annual Conf. on Cold Fusion, The Science of Cold Fusion*, Como, Italy, Societa Italiana di Fisica, Bologna, Italy, 1991.
[155] T.A. Chubb and S.R. Chubb, Bloch-symmetric fusion in PdD_x, *Fusion Technol.* **17** (1990) 710.

[156] P.L. Hagelstein, Coherent fusion theory, *J. Fusion Energy* **9** (1990) 451.
[157] P.L. Hagelstein, Lattice-induced atomic and nuclear reactions, *Proc. Fourth Int. Conf. on Cold Fusion*, sponsored by EPRI and the Office of Naval Research, December 1994.
[158] P.L. Hagelstein and S. Kaushik, *Neutron Transfer Reactions*, *Proc. ICCF-4.*
[159] P.L. Hagelstein, Coherent and semi coherent neutron transfer reactions III, *Fusion Technol.* **23** (1993) 353.
[160] P.L. Hagelstein, I. Chaudhary, M. Melich and R. Johnson, A theoretical formulation for problems in condensed matter nuclear science. in *ICCF-14 Int. Conf. on Condensed Matter Nuclear Science,* 2008, Washington, DC. P.L. Hagelstein and I. Chaudhary, Models relevant to excess heat production in Fleischmann–Pons *Experiments, in Low-Energy Nuclear Reactions Sourcebook*, J. Marwan and S. Krivit (Eds.), 2008, Oxford University Press, Oxford.
[161] M.R. Swartz, Phusons in nuclear reactions in solids, *Fusion Technol.* **31** (1997) 228–236.
[162] M.R. Swartz and G. Verner, Bremsstrahlung in hot and cold fusion, *J New Energy* **3** (4) (1999) 90–101.
[163] M.R. Swartz and G. Verner, Metamaterial function of cathodes producing hydrogen energy and deuteron flux, *Proc. ICCF-14* (2008).
[164] M.R. Swartz, Deuterium production and light water excess enthalpy experiments using nickel cathodes, *J. New Energy* **1** (3) (1996) 219. www.iscmns.org/FIC/J/JNE1N3.pdf.
[165] M.R. Swartz, possible deuterium production from light water excess enthalpy experiments using nickel cathodes, *J. New Energy* **3** (1996) 68–80.
[166] A. Widom and L. Larsen, Ultra low momentum neutron catalyzed nuclear reactions on metallic hydride surfaces, *Euro. Phys*. J. C (2006).
[167] D.P.E. Dickson and F. Berry, *Mossbauer Spectroscopy*, Cambridge University Press, Cambridge, UK, 1983.
[168] L. Eyges, Physics of the Mössbauer effect, *Amer. J. Phys*. **33** (10) (1965) 790–802.
[169] H. Frauenfelder, *The Mössbauer Effect*, W.A. Benjamin, 1962, LCCN 61018181.
[170] T.C. Gibb, *Principles of Mössbauer Spectroscopy*, Chapman and Hall, London, 1974.
[171] J. Hesse, Simple arrangement for educational Mössbauer-effect measurements, *Amer. J. Phys.* **41 (**1973) 127–129.
[172] R.L. Mössbauer, Kernresonanzfluoreszenz von Gammastrahlung, in Ir191, *Zeitschrift für Physik* A (in German) **151** (2): 124–143.
[173] F. Ninio, The forced harmonic oscillator and the zero-phonon transition of the Mössbauer effect, *Amer. J. Phys*. **41** (5) (1973) 648–649.
[174] U. Gonser, *Mössbauer Spectroscopy*, Springer, NY, 1975.
[175] G. Vandergrift and B. Fultz, The Mössbauer effect explained, *Amer. J. Phys*. **66** (7) (1998) 593–596.
[176] T.-H. Han, J.S. Helton, S. Chu, D.G. Nocera, J.A. Rodriguez-Rivera, C. Broholm and Y.S. Lee, Fractionalized excitations in the spin liquid state of a kagome lattice antiferromagnet, *Nature* **492** (2012) 406–410.
[177] F. Monticone and A. Alu, Metamaterial lasmonic and nanophotonic devices, *Rep. Progr. Phys*. **80** (3) (2017).
[178] A. Zvyagin, Parametric pumping of the two-dimensional quantum spin liquid, *Phys. Rev*. B **95** (2017) 064428.
[179] S. Karimi, F. Baboux, F. Perez, C.A. Ullrich, G. Karczewski and T. Wojtowicz, Spin precession and spin waves in a chiral electron gas: beyond Larmors theorem, *Phys. Rev.* B **96** (2017) 045301.